Master thesis and internship[BR]- Master's thesis : Identification of tensions in cross-cables network[BR]- Integration Internship

Auteur : Valentiny, Damien
Promoteur(s) : Denoel, Vincent
Faculté : Faculté des Sciences appliquées
Diplôme : Master en ingénieur civil en aérospatiale, à finalité spécialisée en "aerospace engineering"
Année académique : 2021-2022
URI/URL : http://hdl.handle.net/2268.2/14375

LIÈGE université
Aerospace &
Mechanical engineering

Master's Thesis

Identification of tensions in cross-cables network

Supervisor:
Prof. Vincent Denoël
Candidate:
Damien Valentiny

Master's thesis carried out by Damien Valentiny to obtain the degree of Master of Science in Aerospace Engineering

University of Liege - Faculty of Applied Sciences

Acknowledgements

Firstly, I would to thank my supervisor Prof. Denoël who followed my work during the whole period and has always been open and present to my interrogations. I would like also to express all my gratitude to the staff of V2i that guides me in the company during the whole period of the work. I think especially about my internship supervisor Ing. Sébastien Hoffait who has been my reference in the V2i company. I think also about Ing. Hüseyin Güner who has always been present, and with whom I made the measurements on the bridge of Milsaucy. I would also like to thank Ing. Edouard Verstraelen who always knew how to answer my many questions. Generally, I would also like to thank all the V2i employees for their good mood and their numerous advice when I needed them. Last, I'd also like to acknowledge the help provided by the Service Public de Wallonie (SPW) which was indispensable for carrying out the experimental measurements on the Milsaucy Bridge.

Abstract

Cable tension monitoring is essential to ensure the continuous safety of cable structures throughout their entire lifetime. The present paper aims at developing a frequency-based identification procedure of the axial forces for a network of two cross-cables with non-negligible bending stiffness anchored to possible flexible supports. Physical models relying on the in-plane and out-of-plane dynamic behavior are presented through a Finite Element Method. The previous results are then compared to the outcomes of an analytical approach for validation purposes. To acquire a first set of observed eigenfrequencies, experimental measurements performed on a reduced scale model of the structural network are carried out. The latter shows during the inverse approach a certain limitation, namely that the bending stiffness of the cable is too small to be accurately identified. However, these measurements allow the validation of the inverse identification approach. To perform these identifications, the use of a non-linear Bayesian regression turned out to be a powerful tool to get overall ranges of estimated parameter values with their own probability to be observed. As second method, the function `fminsearch` from the optimization toolbox of `Matlab` proves to be effective in the identification strategy to obtain a single optimal value of the unknown parameters. The use of the Laplace approximation allows to complete this last method by providing a Gaussian PDF around the optimal value. Finally, the validation of the identification method is achieved through the experimental natural frequencies acquired on one selected cable network on the Milsaucy bridge in Liège, leading among other things to the consideration of flexible anchor supports.

Keywords: cross-cable network, vibration-based method, inverse identification approach, tension monitoring, FEM, Metropolis-Hastings algorithm, natural frequencies.

Contents

Chapter 1

Introduction

1.1 Context and motivations

Cable elements play an important role in the field of civil engineering in a wide range of structures of all kinds. They are often considered as the main support elements in bridge applications such as cable-stayed bridges, suspension bridges, tied-arch bridges, or even pedestrian walkways but also for many other applications for stability purposes such as guyed pylon or bracing techniques in the building industry.

In most general cases, its main role is to sustain the applied load on a structure by achieving high levels of tension. In lots of applications, cable becomes the main stressed member of the structure and its health status can therefore directly affects the safety of the structure. Cable damage induced by fatigue, corrosion or others reasons may lead to catastrophic and irreversible accidents. In 2018, for instance, the stayed-bridge of Lixhe in Liège has suffered a lifting of more than 50 cm due to the rupture of a connecting rod, as illustrated in Fig.(1.1). Cable tension monitoring becomes therefore vital to ensure the continuous safety of the structure. It allows to prevent some potential damage caused by an unusual redistribution of forces.

Figure 1.1: Lifting of the Lixhe Bridge (Liège) (URL link , visited in: May, 2022.)

Several methods can thus be performed to assess cable tension. Among them, we can distinguish two different methods of identification.

The first one consists of direct identification by using instrumental devices such as strain gauges or even by using technical approaches such as the measurement of cable elongation. The second method is indirect identification through natural frequencies measurements of the cable network. This method allows a non-intrusive and relatively cheap identification technique since it only requires accelerometers that can be easily placed directly on the structure. To complete the identification approach, a model that directly relates the natural frequencies to the tension must be built. An optimization procedure is then carried out to find the best tension value that minimize the error between the observed frequencies and the ones obtained through the model.

Therefore, one of the key point is to obtain a model that is as adequate as possible, taking into account all the particular conditions encountered in practice. Lots of different models have already been developed in the literature, including: a) the classical taut string model [3], b) cable models including bending stiffness effect, assuming negligible sagging and axial extensibility effects [6], c) models accounting for bending stiffness, and effects due to cable sagging and axial extensibility [2].

In most cases, cable is considered as a straight and unstretchable 1D element due to small values of sag-to-span ratio and of the Irvine's parameter λ^2 [4]. In that way, sagging and axial extensibility effects are assumed negligible. However, even with small values of the bending stiffness, the vibration behaviour of cable structure can radically changed. Neglecting bending stiffness in a model can thus lead to unacceptable inaccuracies in the tension identification procedure. In practise, the values of the bending stiffness is difficult to estimate due to the complex internal geometries of cable element. The bending stiffness

thus usually becomes an additional unknown parameter in the identification problem.
Boundary conditions need also to be modeled with care. Anchorage supports of cables are often assumed as idealized supports, in the form of either perfectly hinged or perfectly clamped which greatly simplifies the analytical models. More realistic models can then be defined by modeling flexible supports in translation and rotation by equivalent springs at the cable end [8].
One of the possibilities to construct the physical model relies on an analytical approach based on the resolution of partial differential equations governing the considered problem. However, the mathematical resolution quickly becomes tricky when more complex cable networks are considered, or when few simplifying assumptions are made. In an alternative way, the use of finite element formulation proves to be an interesting approach to model the dynamics behaviour of cable structure.
The present paper has thus the objective to further broaden these studies by considering news structural schemes using a finite element approach. Those schemes consist of a two crossed cables network having two sub-spans each and partially anchored by flexible supports. Within this context, a first validation of the method is presented thanks to a reduced-scale model of the cable network in different configurations. On-site experimental measurements have been also carried out on the Milsaucy Bridge of Herstal in order to apply the developed method to the identification of tension in the concerned stayed cables.

1.2 State of the art

1.2.1 Direct measure method

Tensiometer

Existing electronic tensiometer using a three points flexion measurements allows a direct identification method of cable tension. Power Limit [Url] is one of the companies that have developed tensiometers able to measure efforts in cables or taut ropes without having to place a dynamometer in line. The company presents a wide range of tensiometers having all their specific applications and limitations in terms of tension values and cable diameter. For instance, the electronic tensiometer with hydraulic assistance HF36/5 [Url] allows to measure more than 40 tonnes with an accuracy of 1% to 5% in cables of 36 to 85 mm diameter. A model of this device is shown in the Fig.(1.2).

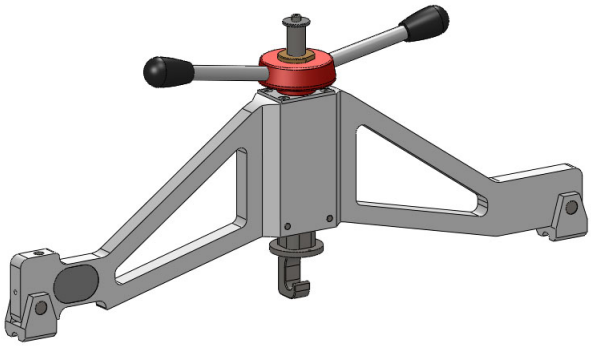

Figure 1.2: Electronic tensiometer HF36/5 from Power Limit (URL)

Although very simple to use, these kind of instruments are not designed for long period of time on site. In consequence, a continuous control of the safety of structure becomes more complex. Moreover, many are the cables where protect layers are present with the help of a sheath made of different materials, such as grease or concrete. The measure of the deformation caused by the three points flexion method can therefore lead to non negligible truncate errors on the tension estimation.

1.2.2 Indirect vibration-based method

The main principle of the vibration-based method is that the cable force is estimated by a set of measured natural frequencies and a specific relationship between the cable force and these frequencies. This method of force assessment is included in the indirect identification method family, as it estimates the tension by measuring indirect physical quantities, which are here the frequencies. The technique has the advantages to provide quick and cheap identification strategies that can be used after the construction stage. The reliability of the method is based on the ability to represent the physical model through the modelling assumptions of the scheme. In particular, the modeling of the anchor supports and the bending stiffness of the cable constitutes perhaps one of the recurrent sources of errors encountered. Existing model already investigated in the literature can be used including or not bending stiffness, sag effect, axial extensiblity effect or flexible supports in rotation and translation. A part of these existing models are briefly presented in the following.

Taut string problem

The transverse vibration of a taut string model is a classical problem that can be found in many vibration and acoustic textbook as an introduction to more complex vibration problems. In the context of this thesis, it could be relevant to have a first review of this simple idealization problem in order to have a better understanding of the concerned full

problem. Let's consider a simply supported cable subjected to a tension T, with mass per unit length m and total length L as represented in the scheme of the Fig.(1.3).

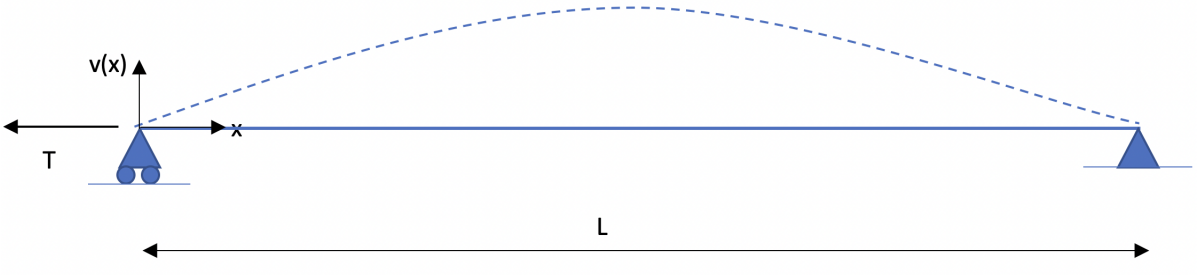

Figure 1.3: Schematic representation of a simply supported cable subject to a tension T

Under the assumptions of a cable without bending stiffness and sagging effect, and considering that the longitudinal displacement is negligible with respect to the transverse motion, the equation of motion for the transverse displacement v writes

$$-T\frac{\partial^2 v}{\partial x^2} + m\frac{\partial^2 v}{\partial t^2} = 0, \tag{1.1}$$

associated to the boundary conditions

$$v(x = 0, t) = v(x = l, t) = 0. \tag{1.2}$$

Let's search for a solution of the 1D wave equation (1.1) of the form

$$v(x, t) = A(x)\sin(\omega t + \phi), \tag{1.3}$$

where $A(x)$ represents the amplitude along x, ω is the circular frequency and ϕ some potential phase shift.
Substitution of this solution in the equation of motion leads to the following differential equation:

$$-TA'' - m\omega^2 A = 0 \tag{1.4}$$

while the boundary conditions become

$$A(0) = A(L) = 0 \tag{1.5}$$

By searching non trivial solutions of the equation (1.4) with the boundary conditions (1.5), the natural circular frequencies of the taut cables writes

$$\omega_n = 2\pi f_n = n\pi\sqrt{\frac{T}{mL^2}}, \tag{1.6}$$

with the normalized associated modeshapes

$$A_n(x) = \sin\left(\omega_n \sqrt{\frac{m}{T}} x\right). \tag{1.7}$$

By measurements of the natural frequencies f_n, the exact value of the associated tension can be directly determined as

$$T = 4mL^2 \frac{f_n^2}{n^2}. \tag{1.8}$$

Bending stiffness considerations

Let's consider now the same problem but with bending stiffness consideration. In most cases, stay cables are characterized by small values of sag-to span ratio and of the Irvine's parameter in such a way that sagging and axial extensiblity effects can be neglected. With these assumptions, the cable can then be modeled as an tensionned Euler Bernoulli beam. The equation of motion for the transverse displacement $v(x,t)$ of the cable subjected to a tension T with length L, mass per unit length m and bending stiffness EI becomes

$$m\frac{\partial^2 v(x,t)}{\partial t^2} + EI\frac{\partial^4 v(x,t)}{\partial x^4} - T\frac{\partial^2 v(x,t)}{\partial x^2} = 0 \tag{1.9}$$

By using the same approach as Furukawa et al. [1], the method of variable separation can be expressed in the form

$$v(x,t) = V(x)e^{j\omega t} \tag{1.10}$$

, where $V(x)$, ω and j represent respectively the modal function, the angular frequency and the imaginary number.
The equivalent ordinary differential equation can then be obtained by substituting equation(1.10) into equation (1.9):

$$-m\omega^2 V(x) + EI\frac{\mathrm{d}^4 V(x)}{\mathrm{d}x^4} - T\frac{\mathrm{d}^2 V(x)}{\mathrm{d}x^2} = 0$$

The general solution of this equation writes

$$V(x) = C_1 \cos\alpha x + C_2 \sin\alpha x + C_3 \cosh\beta x + C_4 \sinh\beta x, \tag{1.11}$$

where C_1, C_2, C_3, and C_4 are the integration constants and α and β are, respectively, expressed as

$$\alpha = \sqrt{\sqrt{\left(\frac{T}{2EI}\right)^2 + \frac{\rho A\omega^2}{EI}} - \frac{T}{2EI}},$$

$$\beta = \sqrt{\sqrt{\left(\frac{T}{2EI}\right)^2 + \frac{\rho A \omega^2}{EI}} + \frac{T}{2EI}}. \tag{1.12}$$

The boundary conditions associated to the simple supports are:

$$\begin{cases} Y(0) = 0 \\ \frac{d^2Y(0)}{dx^2} = 0 \\ Y(L) = 0 \\ \frac{\mathrm{d}^2Y(L)}{\mathrm{d}x^2} = 0 \end{cases} \tag{1.13}$$

Substituting (1.11) in the set (1.13), the four equations for the integration constant C_1, C_2, C_3 and C_4 are obtained. To avoid solution where $V(x)$ is always zero, the equation

$$\sin \alpha L = 0 \tag{1.14}$$

must hold.
The natural frequencies f_n satisfying (1.14) are thus the solution of the discrete equations for the mode number n

$$\begin{aligned} &\alpha_n L = n\pi, \\ &\alpha_n = \sqrt{\sqrt{\left(\tfrac{T}{2EI}\right)^2 + \tfrac{m(2\pi f_n)^2}{EI}} - \tfrac{T}{2EI}}, \end{aligned} \tag{1.15}$$

to finally obtain

$$f_n = \frac{\pi}{2L^2}\sqrt{\frac{EI}{m}}n^2 + \frac{1}{2L}\sqrt{\frac{T}{m}}n. \tag{1.16}$$

The bending stiffness bring therefore a quadratic evolution of the frequencies along the modes. In most cases, the value of the bending stiffness constitutes an additional identification parameters due to the complexity to assess its values in cable structure. However, if the natural frequencies of this model are known, the tension and the bending stiffness can be estimated thanks to the equation(1.16).

Flexible supports considerations

In most cases, anchorage supports of cable cannot be considered as perfectly fixed in translation and perfectly free in rotation in such a way that flexible supports modelling are more adapted. This can be done by introducing equivalent springs in rotation and translation at the boundaries. However, the values of these equivalent springs are often complex to define. They are strongly dependent on the way the cable is anchored, which can vary greatly from one design to another. Different sources of uncertainties are also linked to their estimations, related to potential geometrical imperfections or a modification

of the conditions in time due to aging. In consequence, the equivalent springs values are added to the unknown parameters of the identification problem.
By considering flexible supports, the previous structural model of the stay cable can thus be represented by the scheme of the Fig.(1.4), where ρ_i and $\rho_i^\star$ $(i = 0, 1)$ are respectively the rotational and translational degree-of-fixity parameters.

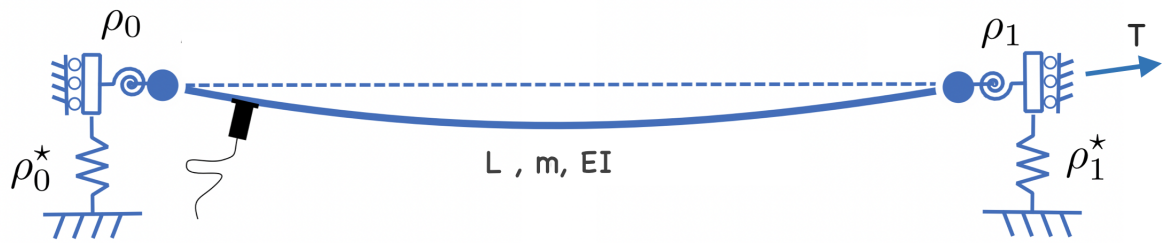

Figure 1.4: Structural model of a stay cable on flexible supports subject to a tension T

Introducing the non-dimensional bending stiffness $\epsilon = \sqrt{\frac{EI}{TL^2}}$ and the characteristic frequency of the taut string model $\omega_0 = \sqrt{\frac{T}{mL^2}}$, the asymptotic expression for the first few natural frequencies can be determined through perturbation methods as,

$$f_n = \frac{\omega_0}{2}\left(n + np\varepsilon + n\left(\frac{\pi^2 n^2}{2} + p^2\right)\varepsilon^2\right) + \text{ord}\left(\varepsilon^3\right), \tag{1.17}$$

where p is a parameter that globally takes into account the flexibility of the supports:

$$p = 2 + \rho_r - 1/\rho_t$$

, with $\rho_r = \rho_0 + \rho_1$ and $1/\rho_t = 1/\rho_0^\star + 1/\rho_1^\star$ [7].

1.3 Considered problem

Cable-stayed bridge are becoming more and more popular in the civil engineering community due to their effectiveness, economic advantages and aesthetic qualities. In most cases, cables become the most important elements in the entire structure due to their high levels of stresses. As spans of cable-stayed bridge continue to be extended, the cable structure becomes lighter, more flexible, and less damped. In this way, excessive vibrations can be encountered, and represent one of the main issues in the health of cable-stayed bridge. Adopted solutions to reduce these amplitudes can be provided by installing external damper [10], or by enhancing cable stiffness by creating cable networks as encountered in bowstring bridge with crossed-lines. This last method shorten the effective length of the connected cables, which would enhance the stiffness of the cable structure. In addition, it was proven that the cross-tie method introduce additional damping to the

concerned cable, and more effective redistribution of the energy through the connected cables. Bridges with crossing cables network, as the one depicted in the Fig.(1.5), becomes thus an interesting kind of structure.

Figure 1.5: Bugrinsky Bridge in Novosibirsk (Russia) [URL link, visited in May 2022]

The objective of this study is to develop an identification method for the estimation of cables force in two cross-cable network. The indirect vibration based method, previously described in the section (1.2.2), is the retained estimation approach due to its high efficiency of identification.

The studied structure is composed of two cables of length L_1 and L_2 crossed by means of a crossed-tie dividing each of its cables into two sub-span with respective lengths l_1, l_2 and l_3, l_4.

The cables are characterized by an uniform bending stiffness EI, a mass per unit length m and are both subjected to tensile force T_1 and T_2. As first approximation, the supports are idealised as perfectly free in rotation, and blocked in the transversal directions.

The considered scheme can be further simplified by splitting the in-plane and out-plane motion, considering them as uncoupled. In the plane of the crossing-lines, the transverse motion can be analyzed by considering each cable separately with the assumptions that, at the crossing point, one cable restraints the transversal displacement of the other through its axial extensibility. This kind of restraint can be simply modeled by a third support blocking all translational displacements. In the out-of-plane direction, the transverse motion of the two cables is considered by making the assumption that the crossing-tie forces the two elements to have the same displacement.

1.3.1 Existing results

D. Piciucco [11] has developed the equations of motion in the plane and the out-of-plane of two cables network simply supported at both ends and with small values of the bending stiffness, leading to the resolution of an eigenvalue problem. To solve the mathematical problem, Piciucco has first used the bisection algorithm with numerical method leading to an almost perfect matching with a corresponding finite element model. However, the concerned numerical method does not provide any direct information on the influence of each parameter on the eigenfrequencies. To counter that issue, an asymptotic second-order accurate closed form equation for the natural frequencies of the cable is presented through a standard perturbation approach. This last helps in understanding the influence of each parameter on the dynamical behaviour of the cable network. However, it has important limitations since this method is valid only for very small values of the bending stiffness. Some of its results will be used as a comparison in the construction of the model.

Chapter 2

Direct analysis

The direct analysis method constitutes the preliminary steps to the identification of tensions in cross-cables. The method consists in determining the natural frequencies of the network, once all the geometric parameters, bending stiffness and tensions are known through a physical model. The construction of an adequate physical model is crucial since it is this one that defines the power of the identification method. In a first step, structural models are developed for both in-plane and out-of-plane transverse motions of the cables network. In a second step, the natural frequencies in the corresponding planes of vibration are solved with the use of a finite element method. A discussion on the influence of different parameters on the eigenvalues solutions is then carried out. Different cases are also studied regarding the modeling of boundary conditions. The obtained results are then compared to Piciucco outcomes [11] using other approaches.

2.1 FEM analysis

The natural frequencies and the corresponding modeshapes of the structure can be determined thanks to a finite element approach. When dealing with long and slender structure where bending resistance is small in comparison with the axial force resistance, truss elements are usually justified. These elements are frequently encountered in practise for long cable-stayed bridge. However, as the cable becomes shorter, even small values of the bending stiffness affect the dynamical behaviour, in such a way that the use of beam element is required. In the considered problem, the effective length of the cables is reduced due to the interconnection between them, amplifying thus the effect of bending rigidity. It is therefore more appropriate to include the bending stiffness parameter EI into the considered problem by treating beam element.
Moreover, the Euler-Bernoulli beam theory seems to be interesting in the application of cables, being slender bodies. This theory is a simplification of the linear theory of elasticity of beam by introducing the kinematic assumptions that the beam cross-section is not deformable, the transverse displacement on it is uniform and the rotation is such that

the cross-sections remain orthogonal to the neutral axis, i.e. the beam does not support shear deformation.

With these assumptions, the internal strain energy over the beam can be expressed as

$$\mathcal{V}_{int} = \frac{1}{2}\int_0^L EI\left(\frac{\partial^2 w}{\partial x^2}\right)^2 dx, \tag{2.1}$$

which implies that the transverse displacement $w(x,t)$ and its first derivative must be continuous. The approximations of the displacement field in the element beam of length l associated to the non-dimensional axial variable $\xi = \frac{x}{l}$ can be written as

$$\begin{aligned} w(\xi) &= w_1\phi_1(\xi) + \psi_1\phi_2(\xi) + w_2\phi_3(\xi) + \psi_2\phi_4(\xi) \\ &= \boldsymbol{\Phi_e}(\xi)\boldsymbol{q}_e(t), \end{aligned} \tag{2.2}$$

where $\psi = \frac{\partial w}{\partial x}$ is the cross-section rotation.

The use of a third-order Hermitian polynomials seems to be adequate to interpolate the bending deflection by ensuring continuity of the displacement and of the cross-section rotation at the nodes.
The kinematic conditions over the element are thus

$$\begin{cases} \phi_1(0) = 1 \quad \phi_1'(0) = 0 \quad \phi_1(1) = \phi_1'(1) = 0 \\ \phi_2(0) = 0 \quad \phi_2'(0) = \ell \quad \phi_2(1) = \phi_2'(1) = 0 \\ \phi_3(\xi) = \phi_1(1-\xi) \quad \phi_4(\xi) = -\phi_2(1-\xi) \end{cases} \tag{2.3}$$

, where $\phi_i' = \frac{d\phi_i}{d\xi}$.

The matrix of shape functions can then be deduced:

$$\boldsymbol{\Phi}_e^T(\xi) = \begin{bmatrix} 1 - 3\xi^2 + 2\xi^3 \\ \ell\xi(1-\xi)^2 \\ \xi^2(3-2\xi) \\ \ell\xi^2(\xi-1) \end{bmatrix}, \tag{2.4}$$

associated to the element degrees of freedom:

$$\boldsymbol{q}_e^T = \begin{bmatrix} w_1 & \psi_1 & w_2 & \psi_2 \end{bmatrix} \tag{2.5}$$

The kinetic energy of a beam element of mass per unit length m and gyration radius r is given by

$$\mathcal{T}_e = \frac{1}{2}\int_0^\ell m\dot{w}^2 dx + \frac{1}{2}\int_0^\ell mr^2\left(\frac{\partial \dot{w}}{\partial x}\right)^2 dx. \tag{2.6}$$

The first term describes the kinetic energy for vertical translation, while the second is the rotational kinetic energy of the cross-sections. As described in [9], the kinematic assumption of no shear deformation remains valid provided that the gyration radius r remains small. The rotational kinetic energy of the cross-section can thus be neglected, so that the kinetic energy at the element level becomes

$$\mathcal{T}_e = \frac{1}{2}\int_0^\ell m\dot{w}^2 dx = \frac{1}{2}\dot{\boldsymbol{q}}_e^T \boldsymbol{M}_e \dot{\boldsymbol{q}}_e, \tag{2.7}$$

with the elementary mass matrix defined as

$$\boldsymbol{M}_e = \ell \int_0^1 m(\xi)\boldsymbol{\Phi}_e^T(\xi)\boldsymbol{\Phi}_e(\xi)d\xi. \tag{2.8}$$

The equation (2.1) can be expressed at the element level by using the local variable ξ to obtain the strain energy over the beam element

$$\mathcal{V}_{int,e} = \frac{1}{2}\int_0^1 EI\left(\frac{\partial^2 w}{\partial \xi^2}\right)^2 \frac{d\xi}{\ell^3} = \frac{1}{2}\boldsymbol{q}_e^T \boldsymbol{K}_e \boldsymbol{q}_e, \tag{2.9}$$

with the elementary stiffness matrix

$$\boldsymbol{K}_e = \frac{1}{\ell^3}\int_0^1 EI(\xi)\left(\frac{d^2\boldsymbol{\Phi}_e}{d\xi^2}\right)^T\left(\frac{d^2\boldsymbol{\Phi}_e}{d\xi^2}\right)d\xi. \tag{2.10}$$

Therefore, for an Euler-Bernoulli beam, the mass and stiffness matrices of the element are respectively:

$$\begin{aligned}
\boldsymbol{K}_e &= \frac{EI}{\ell^3}\begin{bmatrix} 12 & 6\ell & -12 & 6\ell \\ 6\ell & 4\ell^2 & -6\ell & 2\ell^2 \\ -12 & -6\ell & 12 & -6\ell \\ 6\ell & 2\ell^2 & -6\ell & 4\ell^2 \end{bmatrix} \\
\boldsymbol{M}_e &= \frac{m\ell}{420}\begin{bmatrix} 156 & 22\ell & 54 & -13\ell \\ 22\ell & 4\ell^2 & 13\ell & -3\ell^2 \\ 54 & 13\ell & 156 & -22\ell \\ -13\ell & -3\ell^2 & -22\ell & 4\ell^2 \end{bmatrix}.
\end{aligned} \tag{2.11}$$

For tensioned cable, a press-stress stiffness matrix must be add in the element beam involving the additional strain energy resulting from the tension T as

$$\mathcal{V}_{g,e} = \frac{1}{2}\int_0^\ell T\left(\frac{\partial w}{\partial x}\right)^2 dx \tag{2.12}$$

By using the expression (2.2), the first derivative in the previous expression writes

$$\frac{\partial w}{\partial x} = \frac{1}{\ell}\frac{d\boldsymbol{\Phi}_e}{d\xi}\boldsymbol{q}_e$$

The resulting strain energy can then be expressed in its general quadratic form as

$$\mathcal{V}_{g,e} = \frac{1}{2}\boldsymbol{q}_e^T \boldsymbol{K}_{g,e}\boldsymbol{q}_e$$

, with the geometric stiffness matrix

$$\boldsymbol{K}_{g,e} = \frac{1}{\ell}\int_0^1 N_0 \left(\frac{d\boldsymbol{\Phi}_e}{d\xi}\right)^T \left(\frac{d\boldsymbol{\Phi}_e}{d\xi}\right) d\xi.$$

The derivative of the shape function matrix is trivially obtained with the expression (2.4) as

$$\left(\frac{d\boldsymbol{\Phi}_e}{d\xi}\right)^T = \begin{bmatrix} 6\xi(\xi-1) \\ \ell\,(1-4\xi+3\xi^2) \\ 6\xi(1-\xi) \\ \ell\,(3\xi^2-2\xi) \end{bmatrix}$$

in such a way that

$$\boldsymbol{K}_{g,e} = \frac{T}{30\ell}\begin{bmatrix} 36 & 3\ell & -36 & 3\ell \\ 3\ell & 4\ell^2 & -3\ell & -\ell^2 \\ -36 & -3\ell & 36 & -3\ell \\ 3\ell & -\ell^2 & -3\ell & 4\ell^2 \end{bmatrix}. \tag{2.13}$$

This geometric stiffness contribution must therefore be added to the linear stiffness matrix (2.11) to complete the element behaviour. Note that for a tensioned cable without bending stiffness, as a taut string, the elementary stiffness matrix is only reduced to the geometrical one. The assembly of all the elements matrices must then be carried out in order to obtain the structural matrices $\boldsymbol{M}_s$ and $\boldsymbol{K}_s$ of the model. The blocked degrees of freedom related to the supports are then deleted in both matrix. Finally, the modeshapes $\boldsymbol{q}_i$ associated to the eigenfrequencies ω_i are solved numerically thanks to the eigenvalue problem

$$\boldsymbol{K}_s\boldsymbol{q}_i = \omega_i^2\boldsymbol{M}\boldsymbol{q}. \tag{2.14}$$

2.2 In-plane model

The transverse in-plane motion of the cables network can be studied by considering a single cable of the net, assuming that the other provides transversal support at the crossing point through its inextensibility. The in-plane structural model can thus be represented with a simply supported cable subjected to a tensile force T, of length L, mass per unit length m, and bending stiffness EI with an intermediate support. This support corresponds to the crossing point restraint, splitting the cable into two sub-spans of length l_1 and l_2 as shown in the Fig.(2.1).

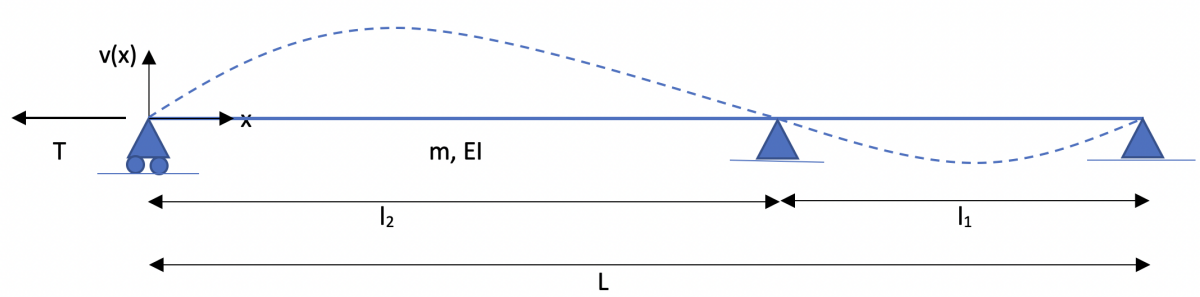

Figure 2.1: In-plane structural model with simple supports.

The natural frequencies and the associated modeshape of the in-plane model can then be determined with the use of the described finite element method of the section (2.1). In order to validate the direct in-plane method, a comparison with the numerical solution of the eigenvalues problem from Piciucco [11] is conducted. For recall, the numerical solution is based on the exact solution of the equation of motion governing the considered problem. Let's consider a cable in accordance with the Fig.(2.1) with the parameters of the Table (2.1).

L [m]	l_1 [m]	l_2 [m]	m [kg/m]	T [kN]	EI $[kN.m^2]$
17.91	12.21	5.7	29.1	1220	230

Table 2.1: Parameters values used for the direct in-plane problem.

The length of the element beam has been set to 28.5 cm after convergence analysis. The first fifteen eigenfrequencies obtained trough the numerical method and the FEM analysis are reported in Fig.(2.2). A regression curve is also represented in order to observe the general evolution of the frequencies. The perfect matching of the natural frequencies with the numerical approach allows thus to validate the finite element model in term of eigenfrequencies computation.
The reliability of the model can also be verified through the shape of the eigenmodes. The first six mode-shapes for the transverse displacement are represented in Fig.(2.3) for both methods.

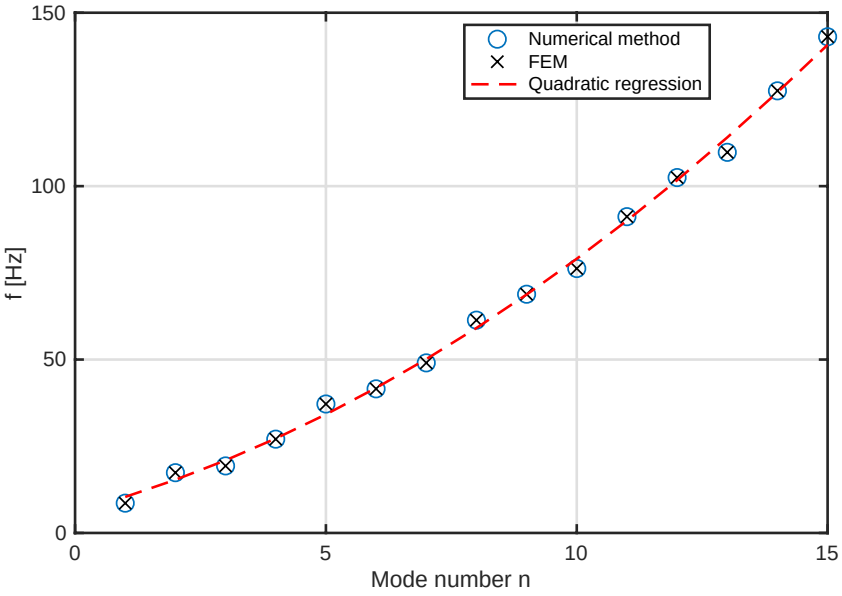

Figure 2.2: Natural frequencies of the in-plane problem obtained with a finite element model and with a numerical model.

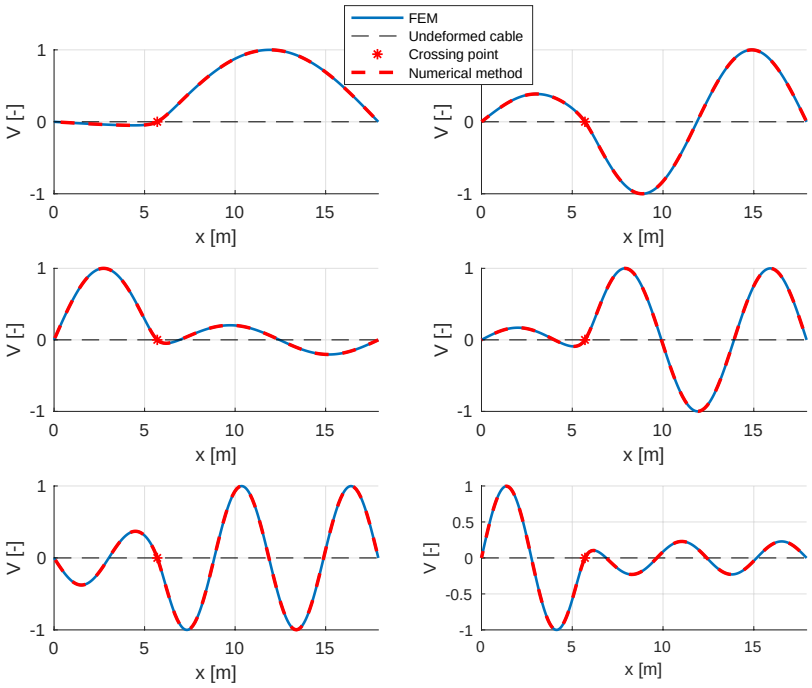

Figure 2.3: Modes shape of the in-plane problem with simple supports obtained with a finite element model and with analytical result.

Once again, the two methods show similar results. Therefore, the dynamical behaviour of the in-plane cross-cable, modeled trough a finite element model as a simple beam with idealized supports can be validated in these conditions.

Influence of the bending stiffness

It could be interesting to see the influence of the bending stiffness on the in-plane dynamical behaviour by considering the cable with negligible bending resistance. This brings us back to the problem of a taut string with an intermediate support that can be easily solved using the vibrating chord theory already introduced in the section (1.2.2). By considering the equation of motion of the in-plane taut-string model with simple supports (cfr.1.1) for each sub-spans, one obtains the decoupled expression of the natural frequencies with respect to both sub-spans of length l_i $(i = 1, 2)$ as

$$\omega_{ni} = \frac{n\pi}{l_i}\sqrt{\frac{T}{m}}, \tag{2.15}$$

while the corresponding normalized modeshapes are

$$V_{n1}(x) = \sin\left(\frac{n\pi}{l_1}(l_2 + x)\right) \quad V_{n2}(x) = \sin\left(\frac{n\pi}{l_2}x\right) \tag{2.16}$$

Consequently, the in-plane modeshapes of a cable with negligible bending stiffness are the combination of the decoupled modes corresponding to each sub-span. In other words, only one of the two sub-spans is mobilized at a given mode number. An exception must be noticed for all integer ratio $k_1/k_2 = l_1/l_2$, where the mode number k_1 and k_2 with respect to the sub-span l_1 and l_2 have the same natural frequencies. In this specific case, the modeshape $k_1 + k_2 - 1$ of the whole structure mobilizes the two sub-spans.

By considering the parameters of the Table (2.1) with null bending stiffness, the natural frequencies can be computed through finite element method adapted for taut-cable (cfr.2.1). The latter method can then be validated with the use of the analytical expression (2.15). Fig.(2.4) illustrates these results.
This time, a linear regression seems to represent the best the evolution of the in-plane frequencies. By comparing Fig.(2.2) and (2.4), one can conclude that bending rigidity brings thus a second order term in the evolution of the natural frequencies of the in-plane problem. This observation is in line with the vibration behaviour of the simply supported cable introduced in section (1.2.2).

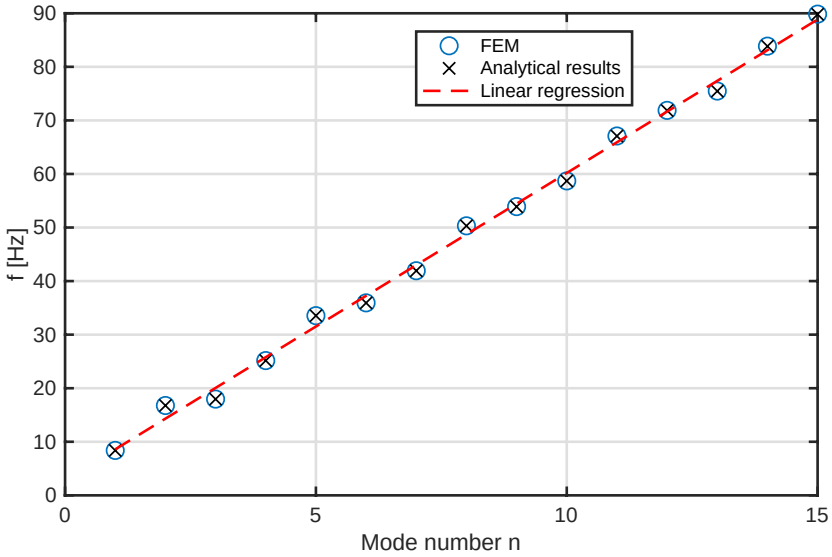

Figure 2.4: Natural frequencies over the mode number of the in-plane taut-string problem obtained with a finite element model and with analytical results.

The first six modeshapes of the in-plane taut string problem can then be visualised using the relations (2.16) and by using the FEM. As expected, the two methods deliver similar results validating once again the approach realized with the FEM.

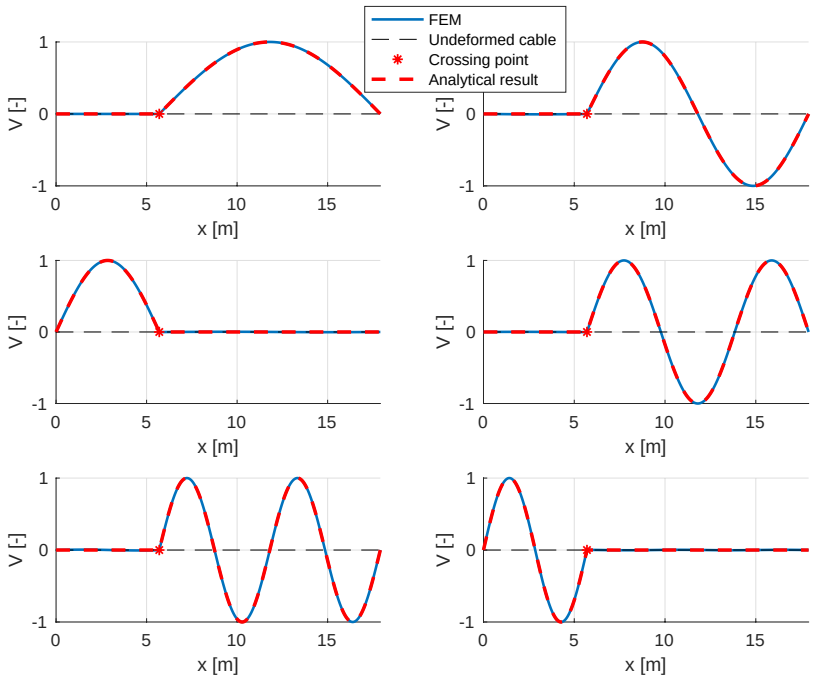

Figure 2.5: Modes shape of the in-plane taut-string problem obtained with a finite element model and with analytical results.

Fig.(2.5) illustrates that without bending stiffness consideration, the modeshapes of the whole structure are the combination of the independent modes of each spans. The order

in which the modes combine is therefore only influenced by the associated wavelength. For instance, the first two modes in the considered problem correspond to the two first harmonics of the right span since its length is more than twice the length of the left span.

By considering in parallel the eigenmodes of the Fig.(2.3), it is clear that the bending stiffness effect brings an additional degrees of connection between the transverse vibration of the two sub-spans. When bending stiffness is considered, the eigenmodes of the left and right spans stay coupled, and the whole system is therefore systematically set in motion.

2.3 Out-of-plane model

The out-of-plane vibration of the cables network can be analyzed considering the two crossed cables of length L_1 and L_2 supported at both ends by simple supports. They are respectively subjected to tensile force T_1 and T_2. The two cables are assumed to have the same mass per unit length m with uniform bending stiffness EI. The first cable is divided in two sub-spans of length l_1 and l_2, and the second cable in two sub-spans of length l_3 and l_4. The attachment point can be seen as a restraint forcing the two cables to have the same displacement. A representation of this conceptual model is shown in Fig.(2.6).

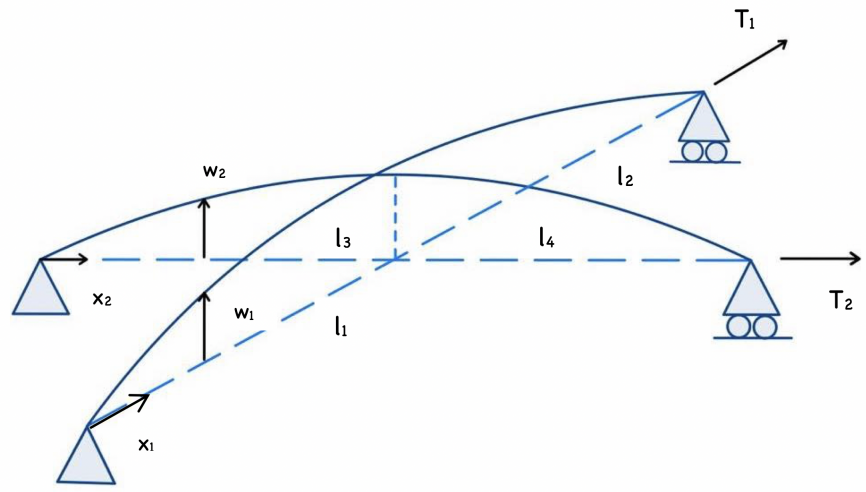

Figure 2.6: Out-of-plane structural model with simple supports.

2.3.1 Eigensolutions analysis

Considering the parameters of the Table (2.2) in accordance with the Fig.(2.6), the out-of-plane eigensolutions can be analyzed with the use of a proper finite element model. The latter method is used by following the description of the section (2.1) and by considering the transversal degrees of freedom at the crossing point identical in both cables. In addition to the FEM solutions, the equations of motion of the out-of-plane problem are solved through a root-finding algorithm as realized in the in-plane problem. This

numerical method, developed by Piciucco [11] and adapted to the considered problem, is presented with the aim of validating the FEM modal analysis.

l_1 [m]	l_2 [m]	l_3 [m]	l_4 [m]	T_1 [kN]	T_2 [kN]	m [kg/m]	EI [$kN.m^2$]
12.21	5.7	5.62	5.07	1220	1750	29.1	230

Table 2.2: Parameters values used for the direct in-plane problem.

Fig.(2.7) illustrates the evolution of the first fifteen eigenfrequencies resulting from the two methods. The observed results allow to conclude that the finite element representation of the out-of-plane simply supported beam is consistent. The natural frequencies are then obtained considering cables with negligible bending stiffness through a FEM for taut-string, and reported in the Fig.(2.7) with the grey data.
Once again, the frequencies of the taut-string problem seems to follow a linear evolution while a quadratic evolution is observed when bending stiffness is considered. This latter brings thus an additional degree in the evolution of the eigenfrequencies, as noticed in the in-plane behaviour.

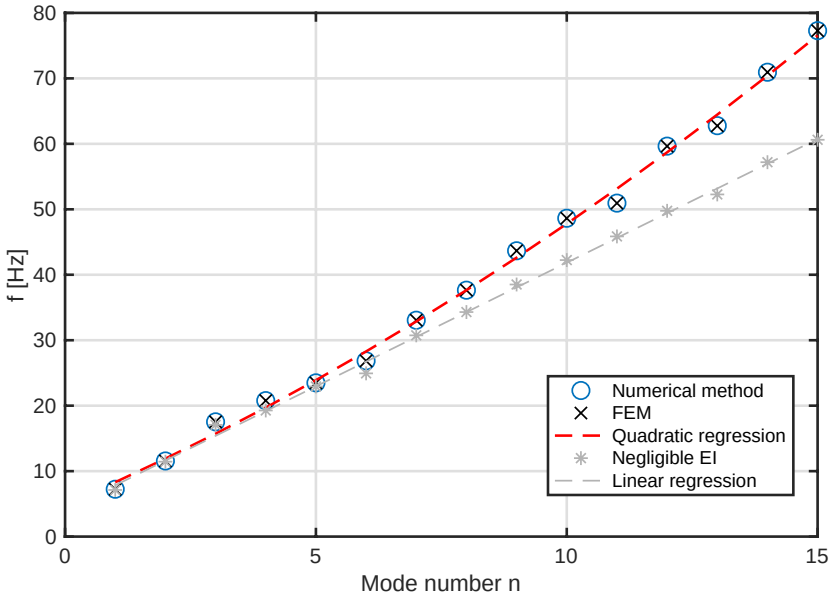

Figure 2.7: Evolution of the frequencies of the out-of-plane cables network with simple supports obtained with a FEM and with a numerical method. The solution for cables with negligible EI is represented in grey thanks to FEM.

The analysis can be further investigated through the modeshapes representation. Fig.(2.8) and (2.9) illustrates these results for the six first modes, where the first cable of the net (with the span 1 and 2) is depicted in the left column while the other one (with the span 3 and 4) is depicted in the right column. A 3D view of the deformed cable is also represented in each sub-figure in which the considered cable is highlighted. The consistency of the

finite element modeshapes is once again approved by the perfect match with the numerical method.

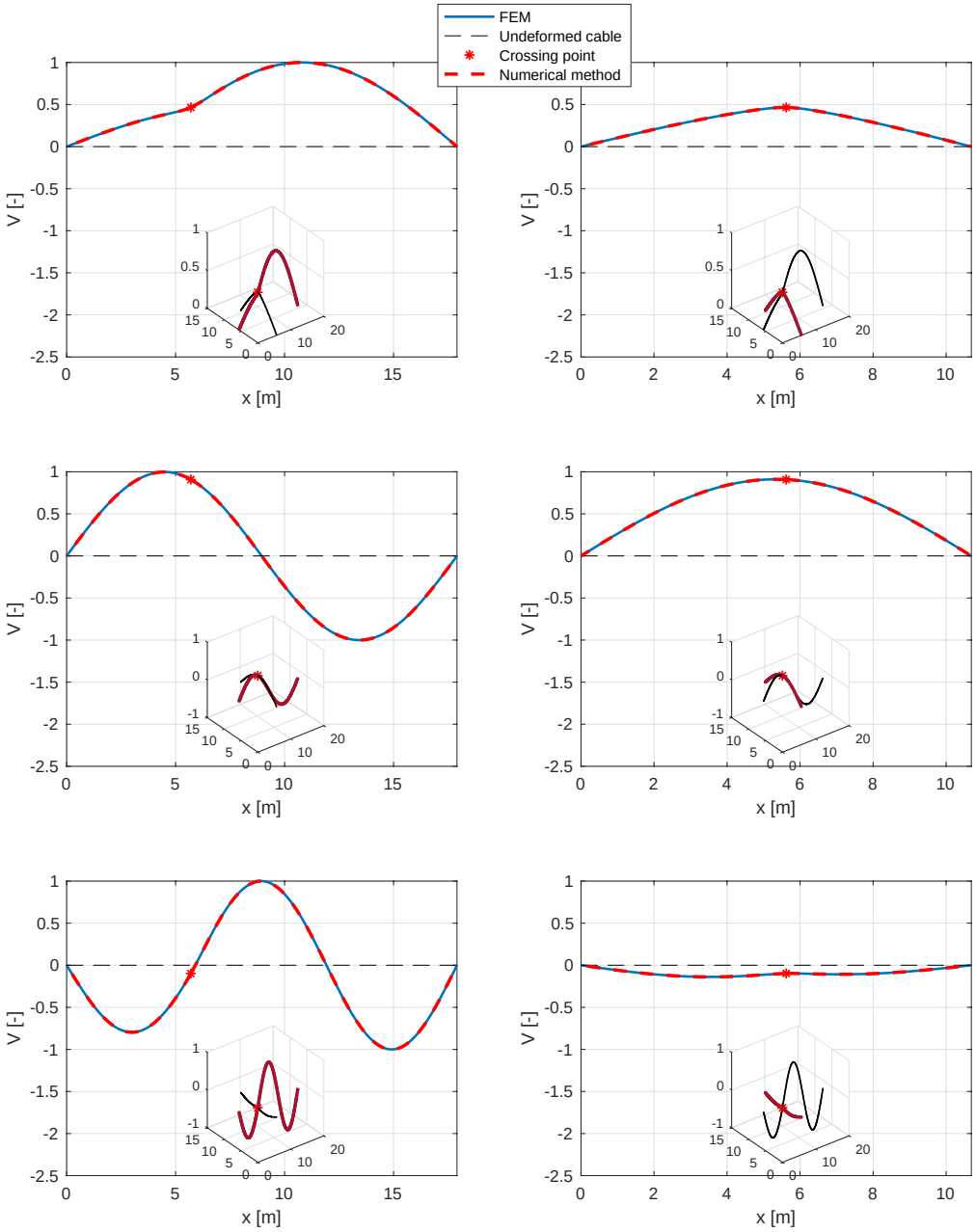

Figure 2.8: Mode-shapes 1 to 3 of the out-of-plane problem with simple supports obtained with a FEM and with a numerical method.

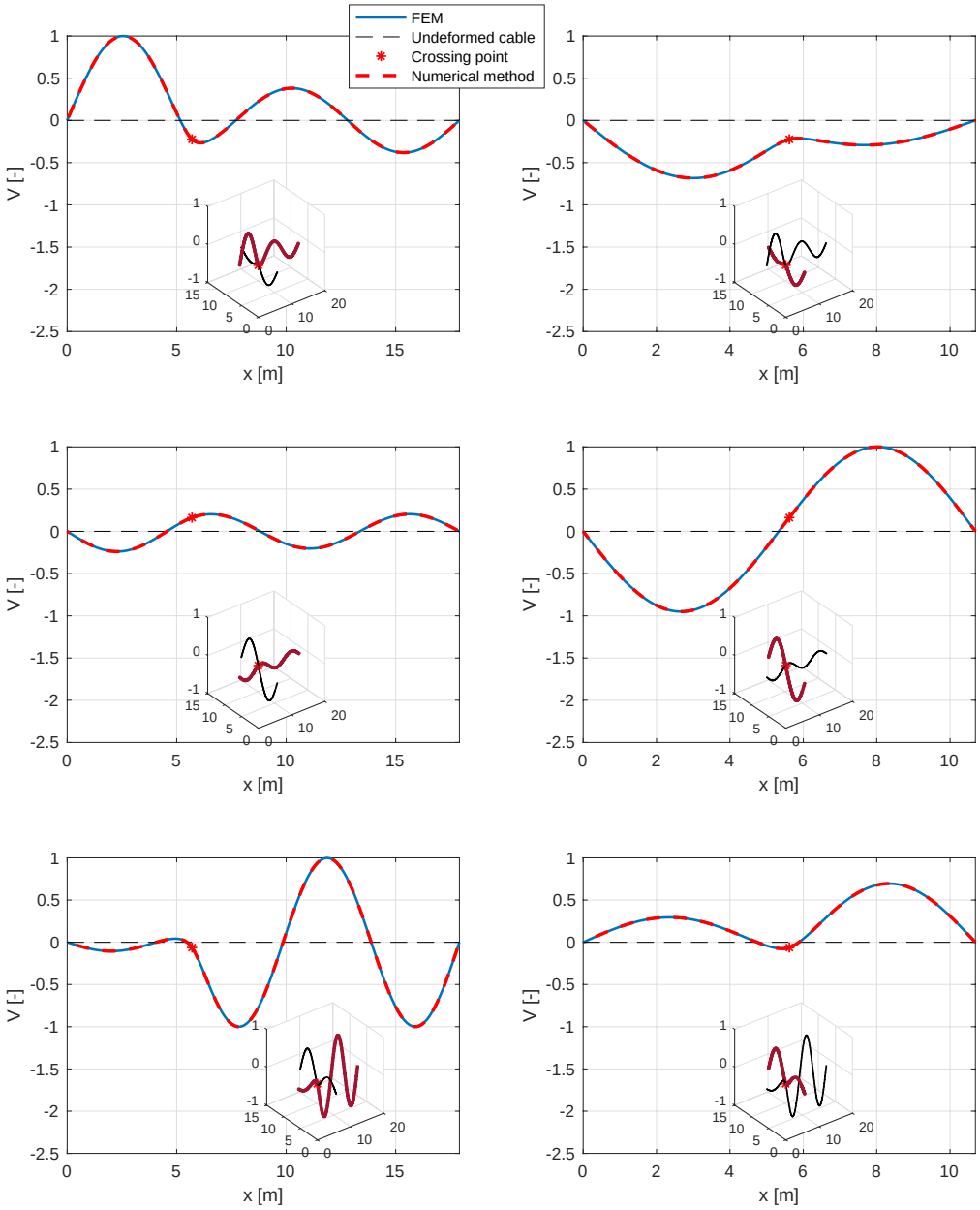

Figure 2.9: Mode-shapes 4 to 6 of the out-of-plane problem with simple supports obtained with a FEM and with a numerical method.

Influence of flexible supports

In most cases, anchor supports of cable cannot be assumed in the form of either perfectly hinged in rotation and perfectly fixed in translation. Flexible supports modeling can thus becomes essential to achieve an accurate identification method. This modeling can be done by introducing equivalent springs at the boundaries as already discussed in the section (1.2.2).

In the context of this thesis, the out-of-plane modeling can be slightly modified by considering flexible supports in translation for two ends section, while the two others are let as perfectly rigid in the transverse direction. In the finite element model, this is simply achieved by adding an additional spring and an additional effective mass in the transverse degrees of freedom of the boundary nodes. The first value corresponds to an effective translational rigidity of the support while the second is an estimation of its displaced mass.
The additional degrees of freedom at the support will only be considered for the out-of-plane problem. Indeed, it is not unusual to observe anchor supports that have non negligible degrees of translation only in one plane of vibration of the cables net. For instance, this kind of support is presented in the Milsaucy Bridge of Herstal as can be seen in the Fig. (2.10), where the anchor is composed of two thin plates, characterized by a bending resistance in the out-of-plane that cannot be assumed infinite. The natural frequencies of the support might thus be in the same order of magnitude as the ones of the cables, creating a coupling between them. In this case, the two ends section of the cables net attached to the ground must be modeled as flexible while the two others can be considered as simple supports in the arch. These assumptions will be validated in the next chapter of this thesis thanks to the collected data on site.

Figure 2.10: Anchor support of the Milsaucy bridge of Herstal.

In order to deeper understand the influence of the equivalent spring value of the support k_s, let's compute the eigenfrequencies of the out-of-plane problem for different values of the ratio $\frac{1}{2\pi}\sqrt{k_s/m_s}$, where m_s is the equivalent mass of the support. Indeed, this ratio can be seen as an estimation of the first natural frequency of the support, allowing thus to directly compare this values to the natural frequencies of the cables network. The Fig.(2.11) shows these results for a characteristic natural frequencies of the support of 20 Hz, 40 Hz and 2000 Hz. One can thus conclude that there exists a coupling between the support and the cables as soon as the characteristic frequency of the support becomes larger than

the modal frequency of the cables. Therefore, for a set of observed eigenfrequencies, the assumption of a rigid support is only valid if the value of this characteristic frequency is larger than the last observed frequency.

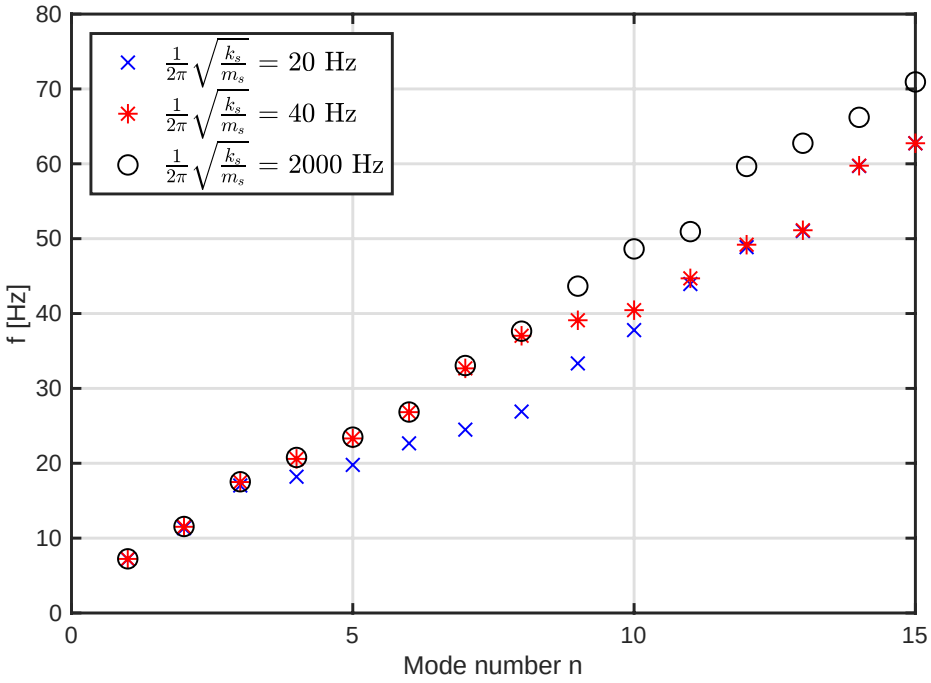

Figure 2.11: Frequencies evolution of the out-of-plane problem of the cables net attached to flexible supports for two ends section and for different ratio of $\sqrt{k_s/m_s}$.

Chapter 3

Experimental measured

The natural frequencies of the cross-lines structure can be further investigated by experimental measured. In the first part of this chapter, reduced-scale models of the structure will be built in the laboratory of V2i company. These set-ups are then analysed to complete the numerical method.
As a first approach, the test model composed of one single cable will be first considered in order to validate some assumptions. As a second step, the natural frequencies of the full cross-line cables will be determined with different configurations to fully understand the influence of each geometric parameters on the dynamic response. The identified frequencies will aim to validate the inverse approach of parameters identification knowing the tension applied to the system.
In the second part of this chapter, on-site measurements are carried out on the Milsaucy Bridge of Herstal. The main purpose of these frequencies measurements will be to identify the tensions in the concerned cables network during the last chapter dedicated to the inverse identification method.

3.1 Reduced-scale model

3.1.1 Test Model

The test model is used to validate some of the assumptions that have been made on the finite element model. In this context, some optional parameters can be adjusted in order to have the best fitting between the model and the experimental set-up. Different parameters are also changed to see their possible influence on the response. The applied tension, the number of the accelerometers and their respective positions on the cable will be the adjustment parameters of the set-up.

Description of the set-up

The test setup assembly consists of a simple steel cable fixed at one end and free at the other where some masses are placed via a pulley. Each support is similar to a totally rigid boundary condition so that the fixed support assumption is consistent. The masses act as control parameters of the tension in the cable. The cable has a diameter of 2 mm, a mass per unit length of 12.5 g/m, and an assumed elastic modulus $E = 185\ 000$ MPa. The length between the support is fixed to 2 m. Given the diameter and length of the cable used, it is expected that the bending stiffness of the cable will be low. It is therefore also expected that the identification of this last parameter on the first identified frequencies will be difficult.

In order to measure the cable natural frequencies, droplet piezoelectric accelerometers are placed near the first support where their weights have only a negligible influence on the dynamics of the cable. This last assumption will be validated in the following. These kind of accelerometers have a sensitivity around 5 mV/g with a frequency range of 5 Hz to 2000 Hz and a mass of 0.5 g. These droplet sensors are then connected to an acquisitor that convert the measure voltage to the corresponding acceleration. The temporal signal and the corresponding frequency response are then directly read on a laptop. The assembly of this set-up can be visualized in Fig. (3.1). For each configuration, an impulse at different places on the cable is made with a hammer.

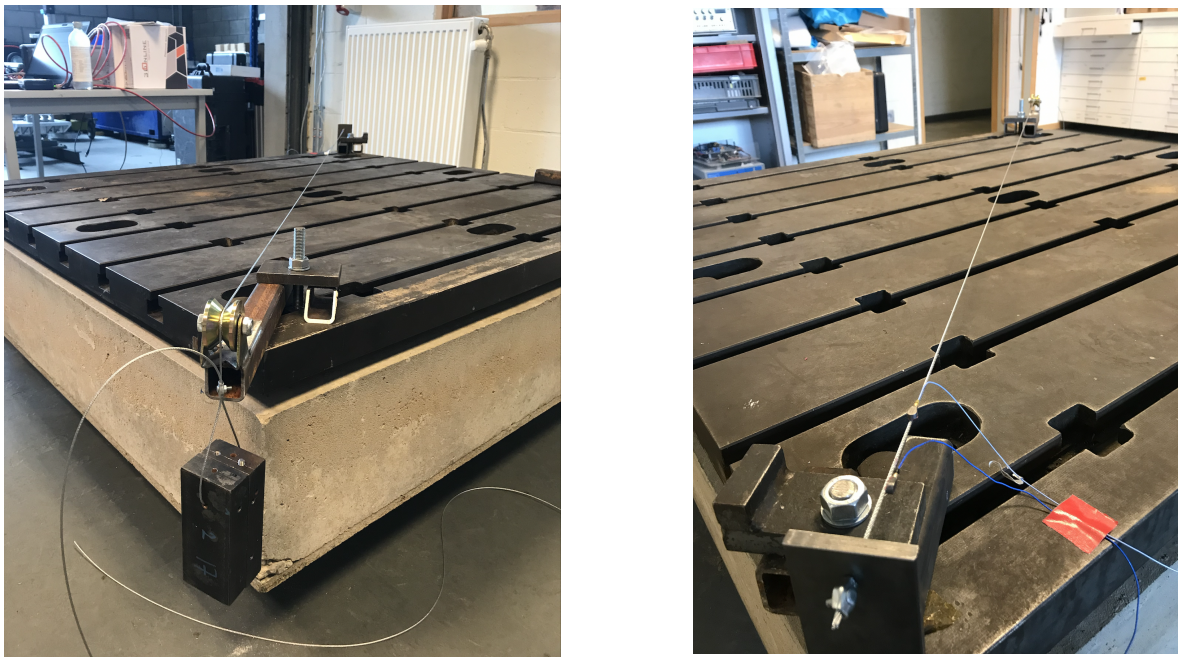

Figure 3.1: Assembly of the test set-up

Influence on the number of accelerometers

It should be interesting to determine the influence of the number of accelerometers placed on the cable. Indeed, an accelerometer can be considered as an additional point mass in the structural model. Fig.(3.2) shows the influence of a 5 g point mass and its position relative to the support on the normalized natural frequencies. This figure is realized thanks to a finite element model of a simply supported taut-string model.

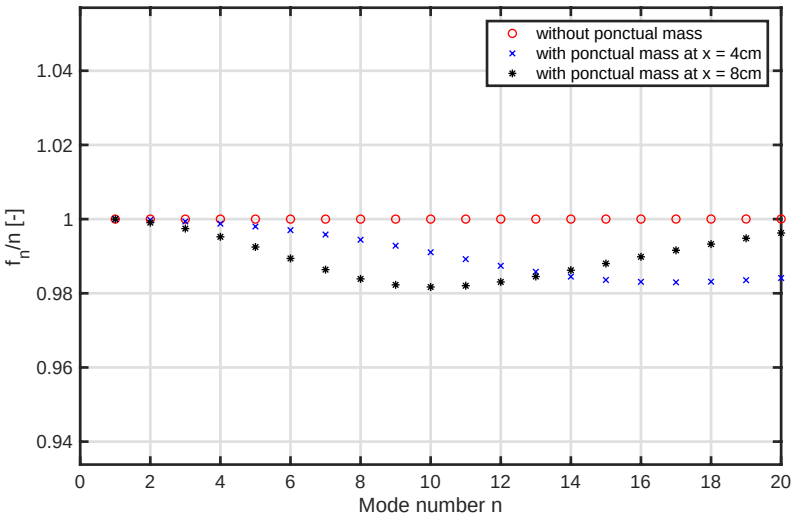

Figure 3.2: Influence of a ponctual mass of 5g in the normalized frequencies over the mode number for a simply supported taut-string (FEM).

The effect of placing an additional inertia in the model generates an overall reduction of the natural frequencies of the system, in the shape of a bucket as observed in Fig.(3.2). The reduction is even more present at low frequencies as the mass moves away from the support. It is therefore interesting to verify if the mass of the sensors used in the laboratory is sufficient to generate a visual modification of the frequency response.

Fig.(3.3) shows time and frequency responses of an impulse realized for a control mass of approximately 10 kg for two cases; one response is obtained by using a single sensor located at 5 cm from the support, the second is realized by placing a second sensor at 8 cm from the support. The acceleration of the cable is acquired during approximately 12 s, allowing a resolution of the frequency response of the order of 0.08 Hz. It might thus be interesting to note that a first source of uncertainty related to the identification of the natural frequencies of the system can be directly linked to this resolution.
These identified modal frequencies are then represented as a function of the mode number for the two cases at the bottom of the same figure. Overall, it can be seen that both frequencies are quietly similar since the relative error between them do not exceed 1%.

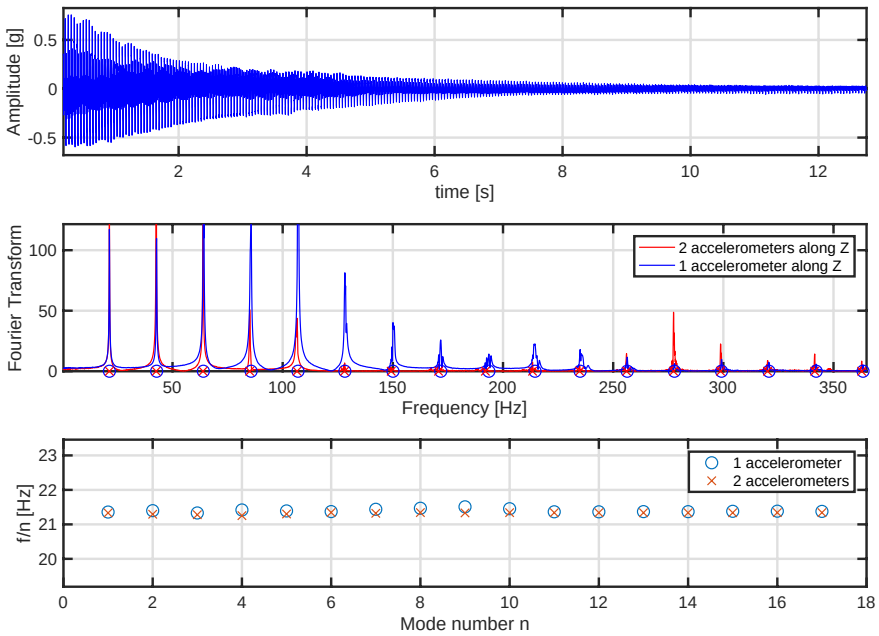

Figure 3.3: Time and frequency responses measured on the test set-up for a control mass of **10kg**.

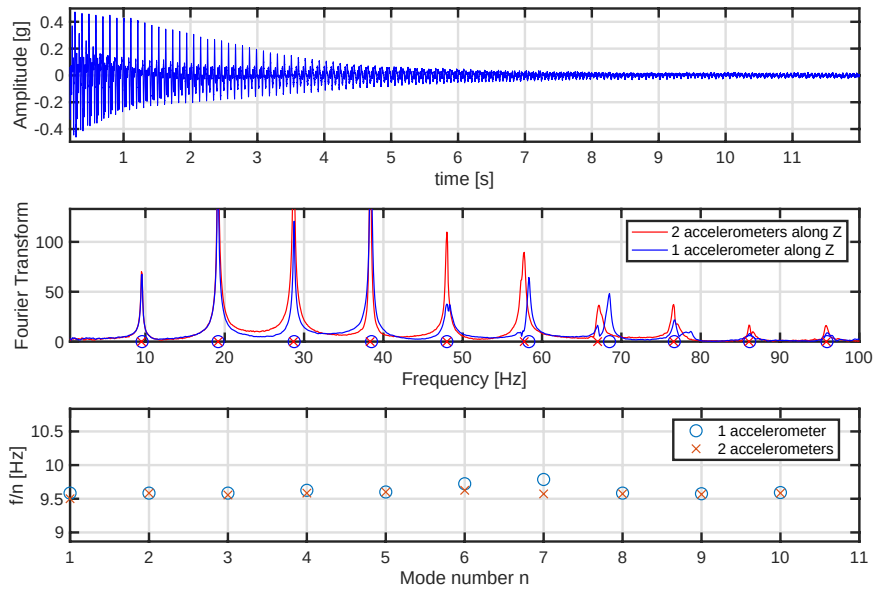

Figure 3.4: Time and frequency responses measured on the test set-up for a control mass of **2kg**

To support these results, the test is repeated with a control mass of 2 kg to see a potential influence of the tension in the cable. As can be seen in Fig.(3.4), the relative errors between the obtained frequencies stay once again below 1%, except for the seventh mode. Indeed, a double peak is presented near the seventh natural frequency of the single sensor solution.

The difference in the identified frequencies is thus linked to a problem of identification of the right peak rather than an additional punctual inertia effect.
These results confirm that there is no influence of the number of accelerometer used on the frequency response as long as the sensors stay close enough to the support.

Influence on the measured direction

It might also be relevant to check that the frequencies associated with horizontal and vertical transverse motions are equal. If verified, the conditions at the supports are similar in both directions, and the cable, once tensioned, can be considered as a perfect isotropic material along its two transverse directions. In addition to that, the assumption of zero sag effect is justified. Fig.(3.5) represents the frequency response of the cable along Z and Y for the set-up configuration with the lowest control tension, i.e. 2 kg, in order to be in the most vulnerable case to this potential difference.

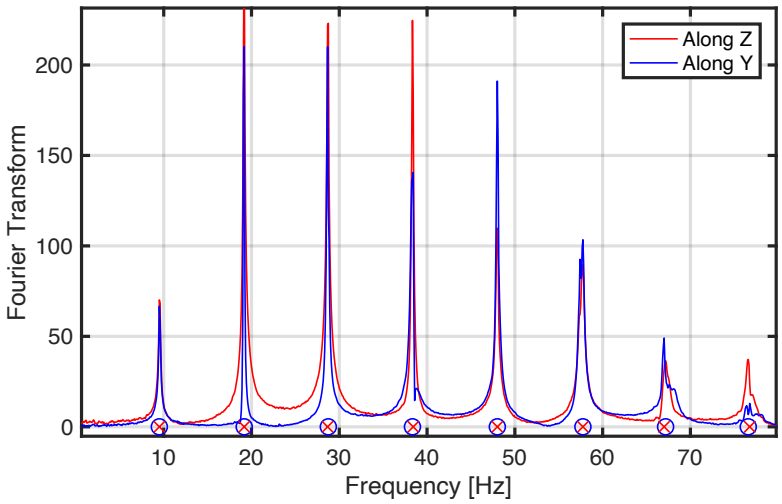

Figure 3.5: Frequency response of the test set-up with a control tension of 2 kg measured along the two transverse directions. The markers represent the identify frequencies in the corresponding directions.

The frequencies along the two transverse directions Z and Y measured by the two sensors may be effectively seen as identical in such a way that the previous assumptions are verified.

An overview of the measured frequencies for three tests realized with a length of 2 m and for a variable control tension of 2 kg, 4 kg and 10 kg are summarized in Fig.(3.6). It seems that the evolution of the frequencies over the mode number follows for each test a constant value, as introduced in section (1.2.2) for the taut-string problem simply supported at both ends.

It is also important to keep in mind that the effect of the bending stiffness is quantified by the non-dimensional parameter $\epsilon = \sqrt{\frac{EI}{TL^2}}$. Regarding this parameter, one can thus conclude that the influence of the bending stiffness on the modal behaviour of one single 2m cable subjected to tension of more than 2 kg is negligible.

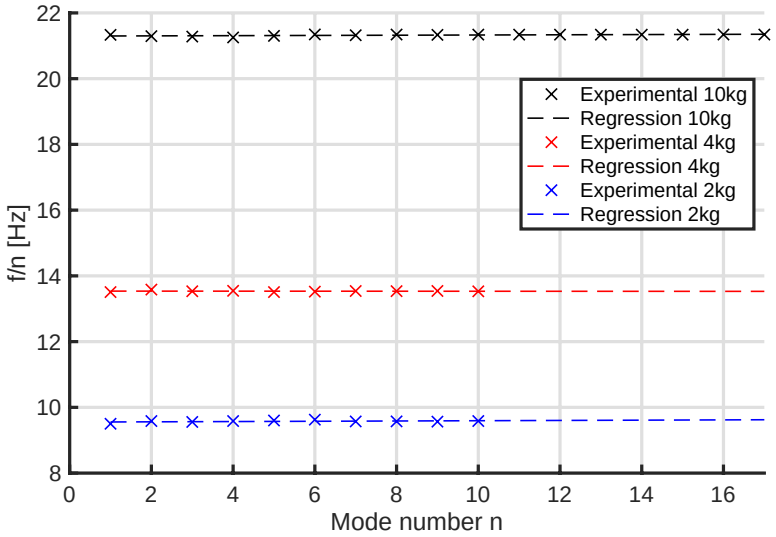

Figure 3.6: Overview of the experimental measured frequencies on the test set-up for control tension of 2 kg, 4 kg and 10 kg and their associated constant regression.

3.1.2 Full set-up

A second cable can then be placed on the previous test set-up in order to complete the full reduced-scale model of the crossed line cables. The supports of the second cable are built in a similar way to the first, i.e. a fixed support at one end and a pulley at the other. The tensions in both cables are once again controlled by the masses attached to the pulley side as observed in Fig.(3.7). The attach between the two cables is built with some flexible metals and consolidate with some plastic clamps as can be seen in right upper corner of Fig.(3.7). This attach restraints the two cables to keep the same displacements. Droplet accelerometers are then placed near the supports in the horizontal and vertical directions depending on the vibration plane to study. The dynamic response is then obtained in similar manner to the test set-up.

Figure 3.7: Assembly of the cross-cables network set-up

A multitude of results are acquired for the horizontal transverse motion of one cable (i.e. the in-plane motion) and for the two cables transverse motion in the vertical direction (i.e. the out-of-plan motion) and this for two different geometrical configurations. The geometrical parameters used for the two configurations are presented in Table (3.1) with reference to the numbering of each sub-span highlighted in red in Fig.(3.7).

	l_1 [m]	l_2 [m]	l_3 [m]	l_4 [m]
Configuration 1	0.97	1.03	0.91	0.99
Configuration 2	0.75	1.25	0.845	0.795

Table 3.1: Length of each sub-span of the full set-up for the two adopted configurations.

In-plane

The in-plane acceleration of cable 1 is measured using two accelerometers placed in sub-span 1 and 2 near their respective end supports. To perform that, a set of impulse excitations are realised in the horizontal direction on each sub-span individually with the use of a hammer. These acquisition tests are then repeated for each geometrical configuration by varying the tensions.
Once all the tests realized, the natural frequencies are identified by comparing separately the frequency responses resulting from an excitation on sub-span 1 and 2. For instance, Fig.(3.8) shows the temporal and frequency responses of each sub-span for an impulse excitation realized on sub-span 1 (right Fig.) and sub-span 2 (left Fig.). The considered test is realized in the first geometrical configuration for a control tension of 4 kg. In this way, the amplitude peaks can thus be clearly identified from these two frequency responses.

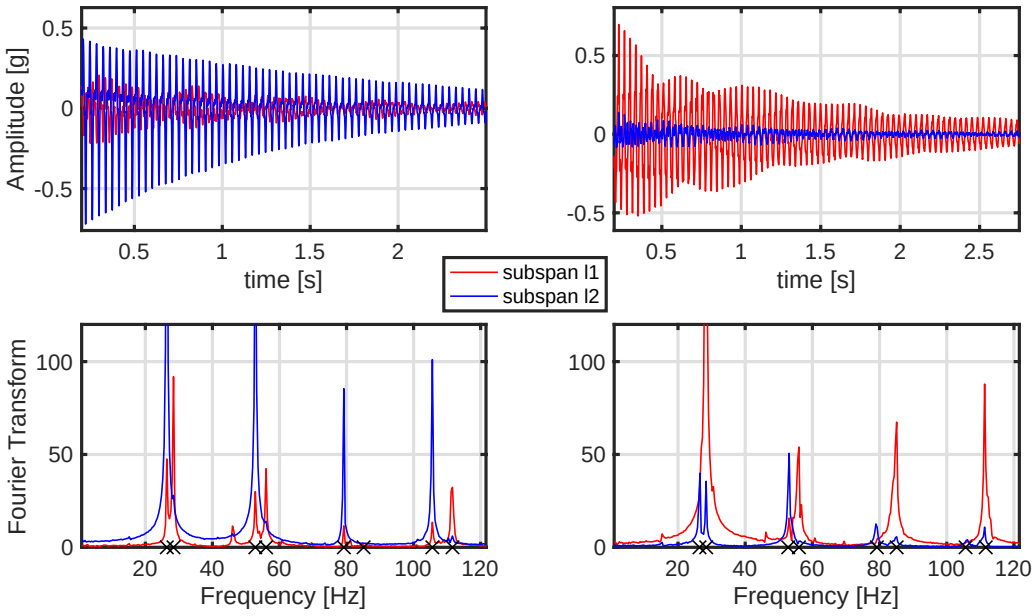

Figure 3.8: Experimental time and frequency responses of the in-plane transverse motion in sub-span l_1 and l_2 in the 1^{st} configuration and for a control tension of 4 kg.

It may be observed in Fig.(3.8) that the natural frequencies are grouped by pairs which is consistent with the length of each sub-span in the first configuration since the first sub-span is slightly shorter than the second one. A continuous alternation is present between

the eigenmodes of the second and first span, thus forming pairs of modes characterized by very close wavelengths. Therefore, each even mode corresponds to the eigenmode of the first span while the odd modes corresponds to those of the second span.

One example of the results obtained for the second geometric configuration is also presented in Fig.(3.9) for a control tension of 8 kg. It is worth noting that the amplitude ratio between the sub-span in each mode is huge. At the first mode for instance, the amplitude in the first sub-span is more than a hundred times larger than the one present in the second sub-span. For the first six modes, this ratio is always larger than seven. These observations result from a weak coupling between the two sub-spans, corresponding to a vibration behavior where bending stiffness effect is negligible.
An interesting observation can also be highlighted in the second configuration at the seventh mode since it corresponds theoretically to a mode where both sub-spans are deformed with equal amplitudes whatever the values of the bending stiffness. At this frequency, the first sub-span presents three vibration antinodes while the second one presents five vibration antinodes since $l_1/l_2 = 3/5$.

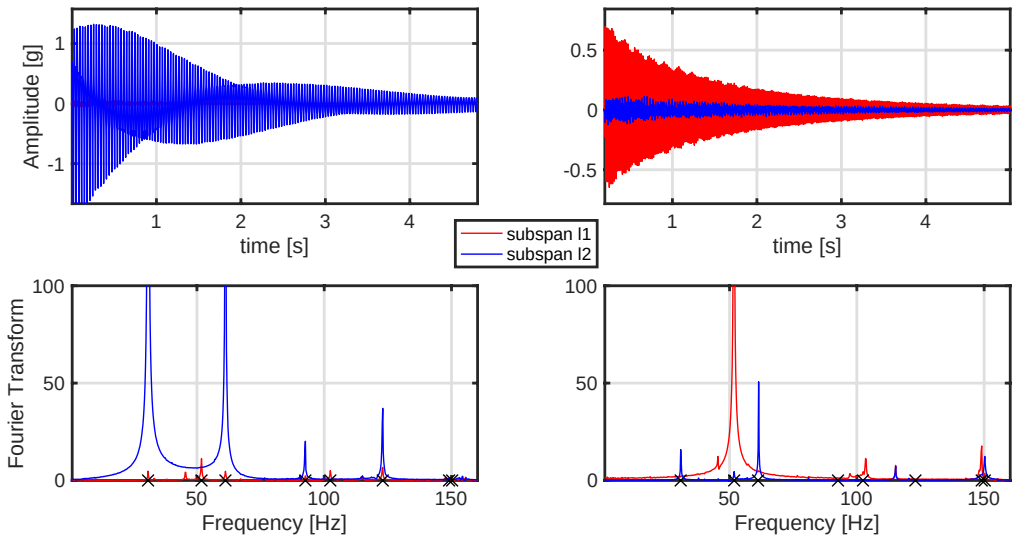

Figure 3.9: Experimental time and frequency responses of the in-plane transverse motion in sub-span l_1 and l_2 in the 2^{nd} configuration and for a control tension of 8kg.

The acquisition part are then carried out in a similar manner to the two previous examples for three different tensions in each geometrical configurations. An overview of the collected natural frequencies of the in-plane set-up is depicted in the Fig.(3.10), where the sub-figures of the left column correspond to the tests realized in the first configuration while those of the right column correspond to the ones of the second configuration.

The influence of the tension presents in the second cable was also studied by making

measurements at constant tension in the first cable for different tensions in the second one. In the first configuration, for instance, the natural frequencies of the first cable with a tension T_1 of 4 kg has been analyzed for different values of T_2 in order to see if there exists a possible interaction between the cables. Fig.(3.10) in the right upper corner shows these results. One could see that a perfecting matching is present between the in-plane natural frequencies of the first cable for the lowest and highest tension (5kg and 9kg) in the second cable, while small differences appears for a tension T_2 of 6 kg. This small gap is however not related to the concerned problem since this tension corresponds to an intermediate value of the two others. To support the results, the test is repeated with a tension T_1 of 7 kg, and for a tension T_2 equals 4 kg and 5 kg in the same geometrical configuration. The lower left corner of Fig.(3.10) allows to observe a very close matching between the identify natural frequencies. Experimental measurements allows thus to show that there is no coupling between the tensions in the in-plane modal behaviour of the crossed-cable network as predicted in theory.

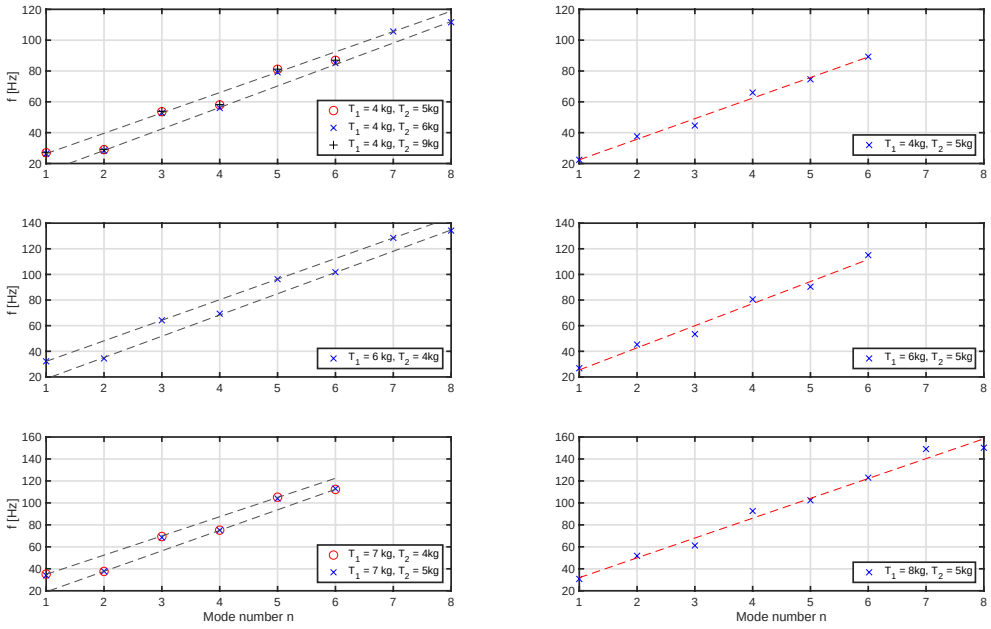

Figure 3.10: Overview of the experimental in-plane natural frequencies for different control tensions. The right column corresponds to the first geometrical configuration while the left column corresponds to the second one.

For each test, a frequency regression curve is used to observe a potential outlier on the set of identified frequencies. A regression line seems to be the most suitable to approximate these first frequencies which is consistent with the low bending stiffness value of the concerned cable. In particular, it is possible to draw two parallel lines in the first configuration since as described above, each odd mode corresponds to an eigenmode of the longest span while the even modes are those of the shortest span. The in-plane problem

can thus once again be likened to the in-plane taut-string problem as analysed in section (2.2).

Out-of-plane

The out-of-plane measurements are then performed using three accelerometers placed in sub-span 1, 2 and 4 in a vertical position. As realised in the in-plane acquisition, three different tensions couples are considered for each geometric configuration.
The identification of the natural frequencies are then determined by looking at the Fourier transform of the three measured responses simultaneously. An example of the temporal response and its respective Fourier transform are depicted in Fig.(3.11) in the second configuration for applied tensions of $T_1 = 6$ kg and $T_2 = 5$ kg. In this figure, one may observed that the three spans present some amplitudes in each of the modes facilitating thus their identification.

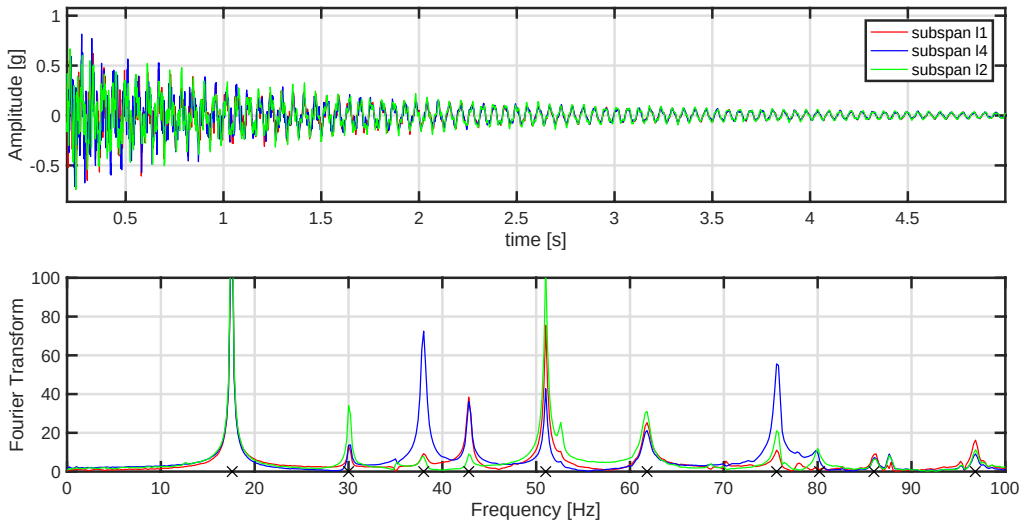

Figure 3.11: Experimental time and frequency responses of the out-of-plane transverse motion in sub-span 1, 2 and 4 in the 2^{nd} configuration and for control tensions of $T_1 = 6kg$ and $T_2 = 5kg$.

The identification procedure is then carried out with similar methods for the five others tests with applied tensions varying from 2 kg to 8 kg. Fig.(3.12) gives an overview of all the collected natural frequencies of the realised tests for the first and second geometrical configuration respectively depicted in the left and right column. As observed in the in-plane problem, a linear regression seems to best fit the observed frequencies leading to a negligible influence of the bending stiffness parameter on these frequencies.

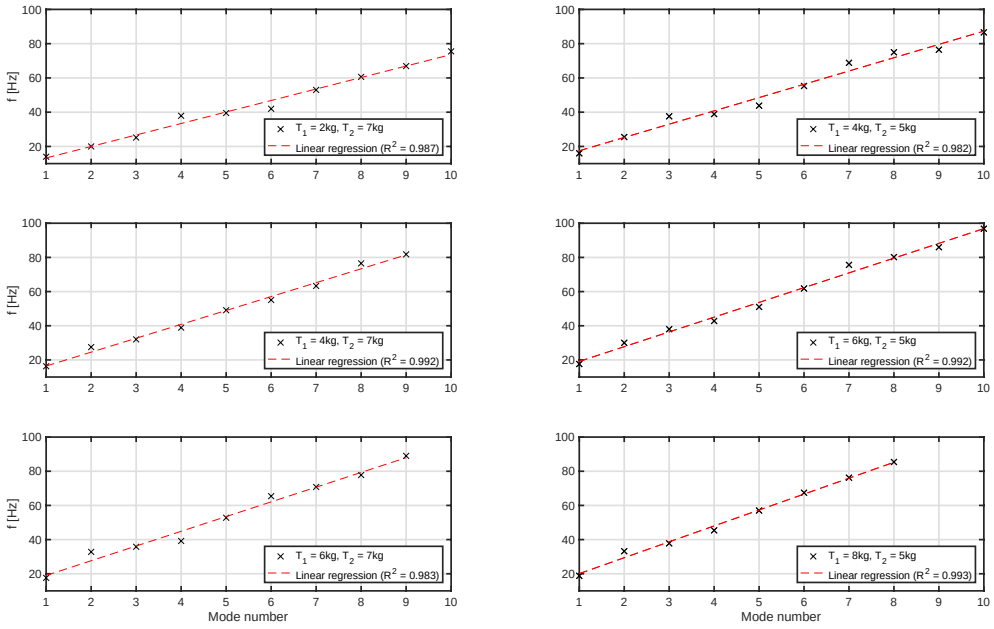

Figure 3.12: Overview of the experimental out-of-plane natural frequencies for different configurations. The left column corresponds to the first geometrical configuration while the right column corresponds to the second one.

3.2 On-site measurement

The dynamical behavior of the crossed line network can be further investigated through measurements on a real bridge. In this part, an acquisition campaign is carried out on the Milsaucy Bridge (Fig.3.13) located at Herstal (Liège) thanks to the partnership with the Public Service of Wallonia (SPW). The collected data will then be compared to the ones predicted by the model to see if the predictions match the on-site measurements.

Figure 3.13: Tested cable-stayed bridge, Herstal (Liège).

3.2.1 Description of the bridge

The Milsaucy bridge is an arch-shaped cable-stayed bridge with a span of 145 meters, a width of 15.5 meters and an arch rise of 23 meters. The arch has tubular rectangular cross-sections of dimensions 1.5 x 1.16 m with a variable thickness along the bridge. The height of both the deck and the arch can be expressed as a parabolic function along the span.

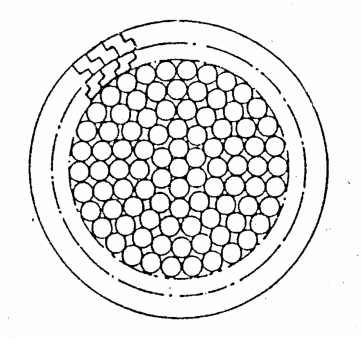

Figure 3.14: Representation of a cable cross-section of the Milsaucy bridge.

The deck of the bridge is connected to the arch by a network of 12 cables with two or three sub-spans. The cables have an external diameter of 75 mm, an equivalent section of 3500 mm^2, and a mass per unit length of 29.1 kg/m. The internal structure of the cable is composed of a multitude of threads of varying diameters as shown in the cross-sections representation of Fig.(3.14). The internal part of the section is composed of 91 clear wires of approximately 5 mm. The term clear wire is used when this one is not sheathed, so it is a simple steel wire. The external part is then sheathed with Z-shaped wires. These are covered with a layer of zinc to protect them from corrosion. The assumed elastic modulus of the cable is $E = 168000MPa$.

The cables are connected to the deck by anchor supports as shown in the right Fig.(3.15). It is composed of two parallel thin plates, characterized by small value of flexural rigidity in the out-of-plane. It is therefore expected to observe non-negligible out-of-plane amplitudes at the supports so that the assumptions of idealized fixed support in translation cannot be verified. Concerning the cross-tie, as depicted in the right Fig.(3.15), this one should prevent any relative motion.

Figure 3.15: Picture of the connector and the anchored support.

3.2.2 Experimental set-up

The objective of the set-up is the measurement of the in-plane and out-of-plane natural frequencies of one of the crossed-cables network present in the bridge. The selected couple of cables is the one located at the end of the right bank of the river on the upstream side. The lengths of each concerned sub-spans are listed in Table (3.2) associated with the numbering in the left Fig.(3.16).
The measurements were performed using some three-directions piezoelectric accelerometers placed on each sub-span approximately at one-third length of the corresponding sub-span as highlighted in Fig.(3.16). Each sensor has the capability of measuring simultaneously the in-plane and out-of-plane transverse motion by placing them beforehand in the right orientation. The accelerometers were then remotely connected to a computer that continuously acquired the response. The time step used for the acquisition is 1/128 s allowing thus to identify frequencies up to 64 Hz.

Two different methods of excitation of the lines were used in each concerning direction. The first one consists of applying a single impact with a hammer at approximately two-thirds of the length of each sub-span. The operation is repeated five times on each sub-span ensuring that the response between each impulse has been dissipated.
The second method of excitation consists in approaching a random excitation by applying impacts in an aperiodic way on the cable continuously for approximately 5 minutes.
Random excitation combining in-plane and out-of-plane response is also achieved by simply leaving the traffic on the bridge free.

In a first configuration, two accelerometers are also placed on the bridge arch; one located in the extension of the smaller cable, the second between the two cables. The natural frequencies and the vibration amplitude of the arch can then be determined to ensure that there is no interaction with the modes of the stays.
In a second configuration, the two previous accelerometers are moved on both anchors of the deck in order to have an estimation of the rigidity of the support in the in-plane and out-of-plane direction. This last configuration will be further discussed in the part dedicated to the validation of the model. The position of all sensors can be visualized in Fig.(3.16).

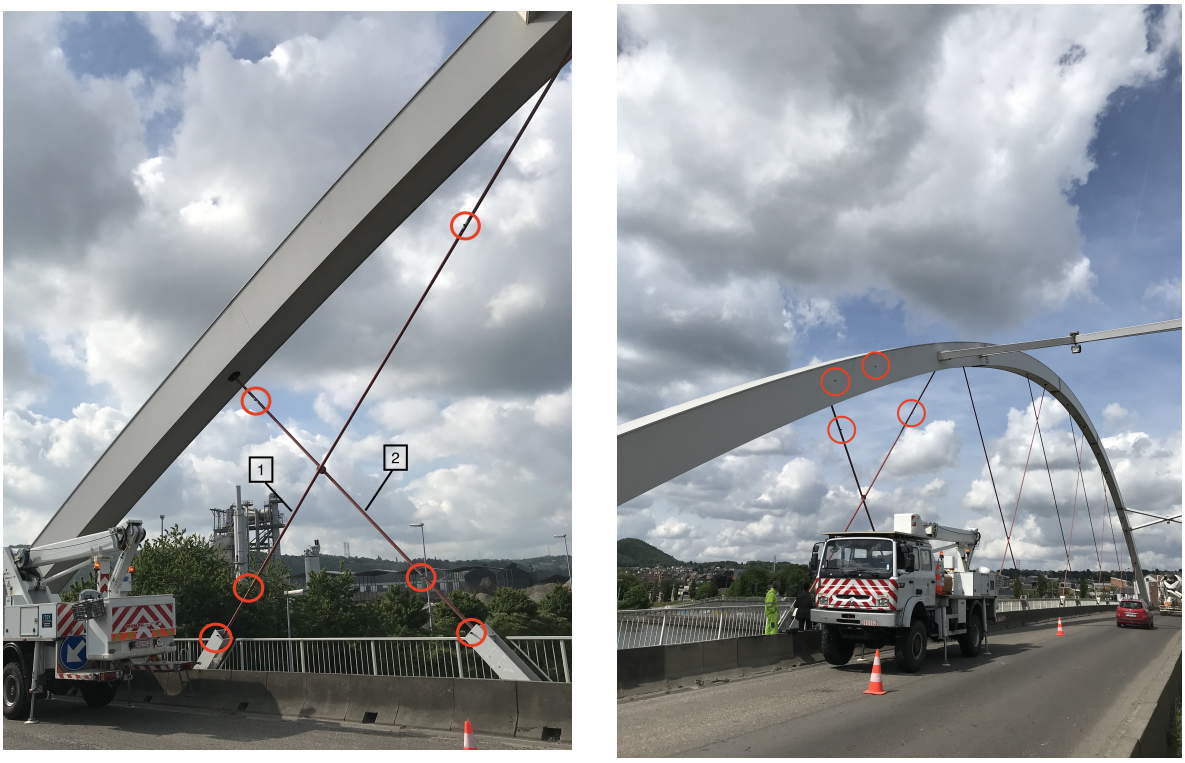

Figure 3.16: Position of the accelerometers highlighted by the red circles and numbering of the two studied cables.

Cable number	Lower span [m]	Upper span [m]	Total [m]
1	5.7	12.21	17.91
2	5.62	5.07	10.69

Table 3.2: Length of the studied cables network

3.2.3 Frequencies identification method

As introduced above, the in-plane and out-of-plane vibrations are initiated a first time with a set of impulse excitation and a second time with random excitation. These two excitations are applied directly on the cable for each vibration plane. It is worth noting that the traffic on the bridge is left free so that additional excitations in the impulse response appear at each vehicle passage.

In this section, the identification of the natural frequency will be carried out to obtain a maximum number of these frequencies. For the random excitation, the full acquisition response will be treated by computing the mean Fourier transform of each signal. For the set of impulse excitation, each of them will be analyzed separately by selecting samples of the full acquisition signal. In that way, only the desired part of the full acquisition is used. The frequency response is then computed for each of these impulses. All the information is then brought together by realizing a mean FFT of all these samples.

The in-plane natural frequencies will be determined with the use of the impulse approach while the out-of-plane frequencies will be presented with both excitation methods.

In-plane

The in-plane vibration response of the first cable of the net is considered with the use of the two accelerometers placed on each of its sub-span. Let's denote the lower span l_1 and the upper span l_2.
A set of six impulses are realised in sub-span l_1 with approximately 30 seconds of interval between each. Fig.(3.17) presents the full acquisition signal of this temporal response in the span l_1 and l_2. Each impulse is then analyzed separately by selecting them from the full signal. Fig.(3.18) shows the five selected samples and their respective frequency responses for both sub-span. From this figure, one may be observed that some modes mainly mobilize only one of the two sub-spans which appear to be the predominant peaks in the frequency response. Other smaller peaks can however be detected mobilizing both sub-spans in the same order of magnitude. These last observations bring thus additional information to the selection of the right mode. Eventually, all the information can then be brought together into a single frequency response by realizing a mean FFT of all the samples. Fig.(3.19) depicts this result.
With the use of Fig.(3.18) and (3.19), the first seven in-plane natural frequencies of the first cable are identified.

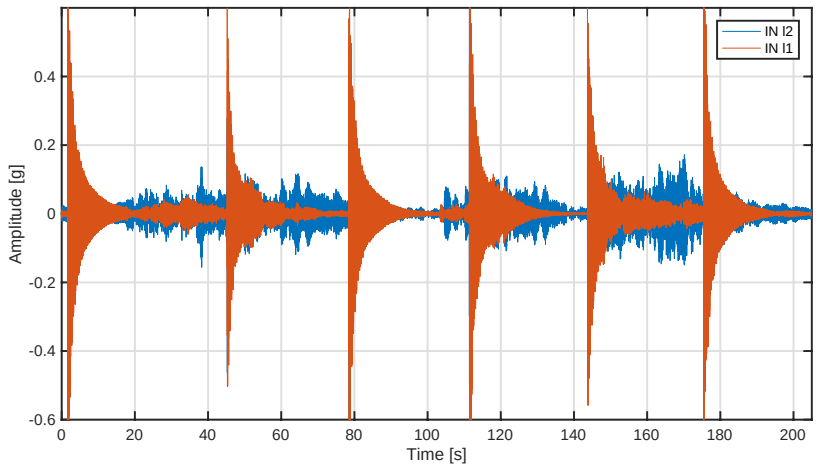

Figure 3.17: Full acquisition over time of the impulse in-plane response realised in the lower span l_1 of the cable 1.

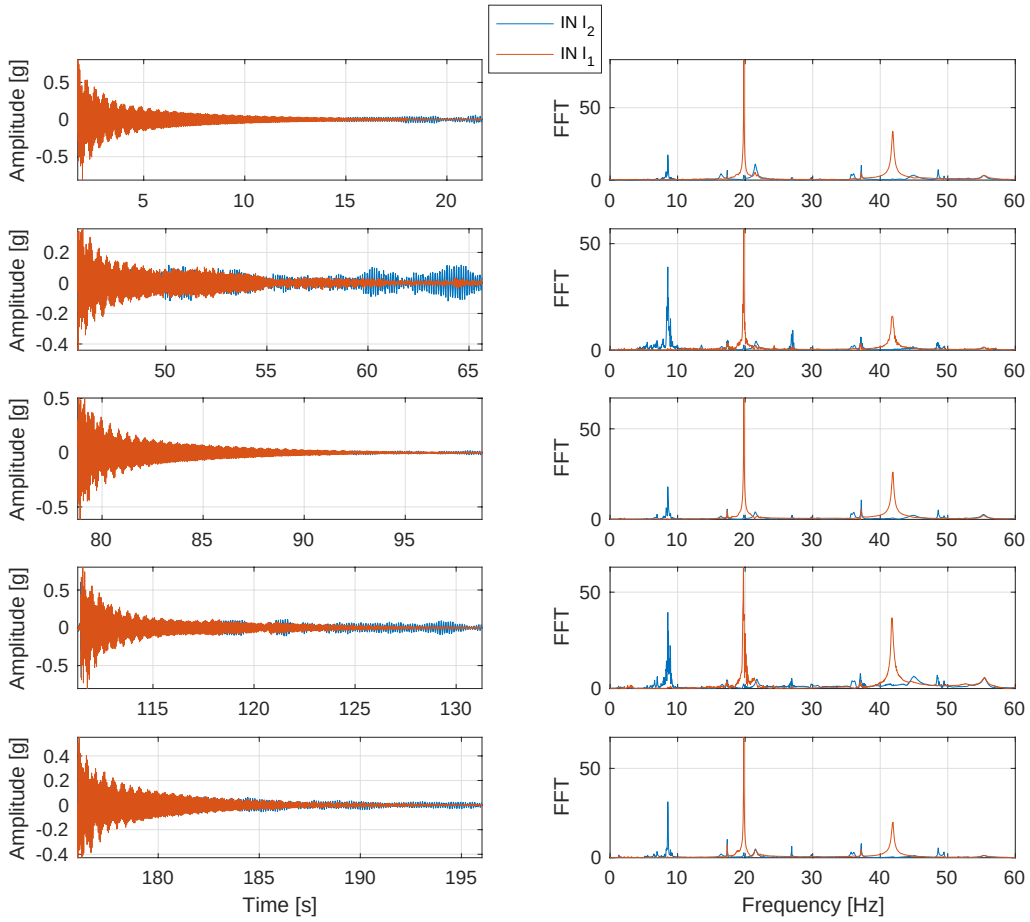

Figure 3.18: Visualisation of each samples from the full acquisition signal of the in-plane problem of the first cable and their respective FFT.

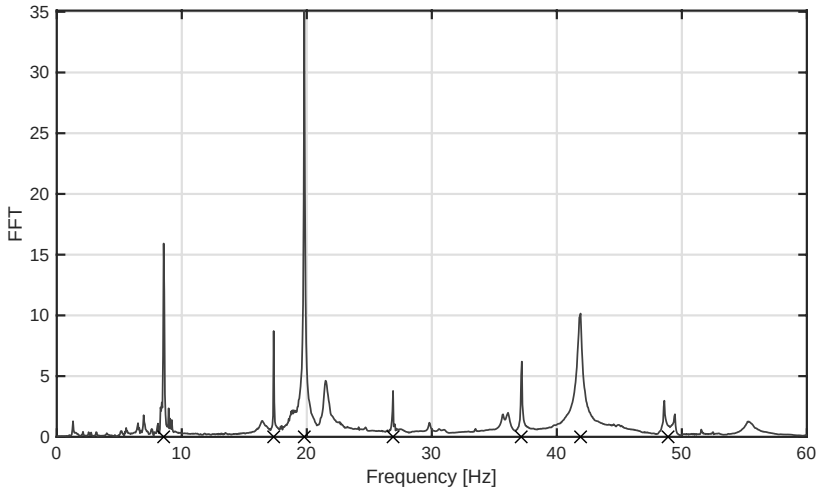

Figure 3.19: Mean FFT of the in-plane first cable response.

By using the same approach as for the first cable, the first four in-plane natural fre-

quencies of the second cable are deduced. Fig.(3.20) shows the full acquisition temporal response and its corresponding mean FFT for the lower and upper spans of the second cable, denoted respectively l_3 and l_4. By looking at the natural frequencies, it seems that the second cable is much stiffer than the first one, allowing thus to identify only four frequencies in the acquisition range.

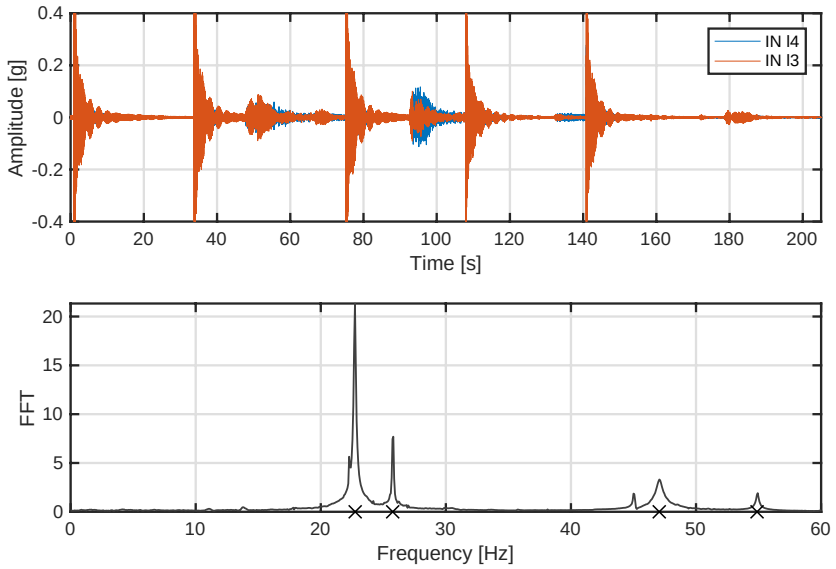

Figure 3.20: In-plane response of the second cable over the full acquisition time for impulse excitation realised in the lower span l_3 and its corresponding mean FFT.

Out-of-plane

The out-of-plane transverse vibration of the net is studied with the use of the four accelerometers placed in the four sub-spans. The corresponding transverse motion is then initiate thanks to a series of impulses realized in the sub-span l_1. The identification of the natural frequencies is then carried out using the same procedure as for the in-plane excitation. The four responses are analyzed separately by sampling the impulses. The frequency responses obtained on each of these samples are then averaged to obtain a single FFT containing all the collected data. Fig.(3.21) presents these final results for all seven pulses performed. From this response, the first thirteen natural frequencies are identified. It is worth noting that the peaks at low frequency are much less present in the response, making their identification more complex. However, the analysis presented in the following section will validate their identification.

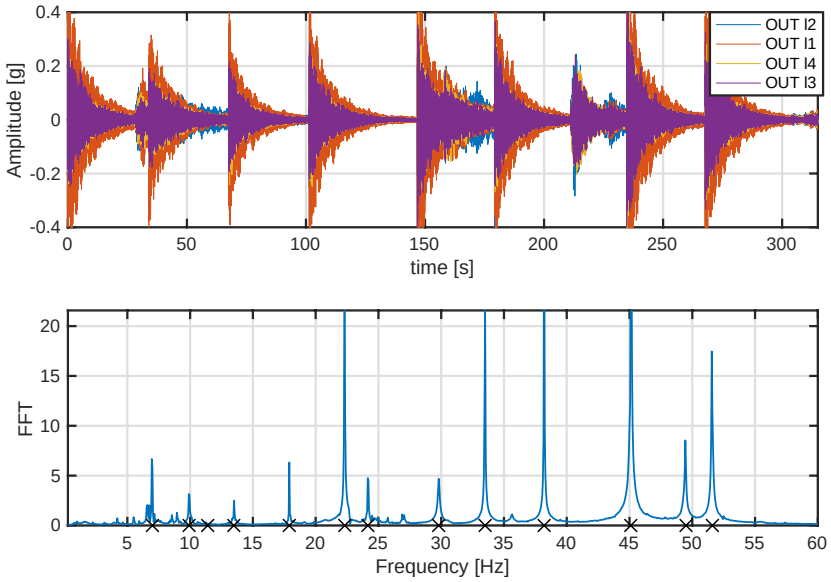

Figure 3.21: Response of the four sub-spans to impulse excitation on sub-span l_1 in the out-of-plane direction and the corresponding mean FFT signal.

3.2.4 Support amplitude consideration

Preliminary consideration

As already introduced in section (2.3), the effect of flexible support on the modal response must be considered if the characteristic natural frequency of the concerned support is in the same order of magnitude than the natural frequencies of the studied structure. This characteristic frequency is directly related to the bending stiffness and the equivalent mass of the anchor support.

These support properties can be approximate with the use of a FEM model. Fig.(3.22) shows a model of the anchor support of the Milsaucy bridge and its static deformation in both direction due to an external force of 1 kN in the concerned direction. This model is developed with the use of the software SIEMENS NX. The equivalent stiffness k_s in both directions is therefore deduced from the deformation amplitude at the point where the cable is fixed (node 6778 in 3.22). The value associated to the out-of-plane transverse motion is therefore equal to $k_{s_{out}} = 682.6$ kN/m while the one associated to the in-plane transverse motion equals $k_{s_{in}} = 102041$ kN/m. The equivalent mass m_s is directly given by the CAO model, this one is approximated to 284 kg. Therefore, the characteristic natural frequency of the out-of-plane transverse motion of the support is given by

$$f_{s_{out}} = \frac{1}{2\pi}\sqrt{k_{s_{out}}/m_s} = 7.8Hz$$

while the one of the in-plane transverse motion is

$$f_{s_{in}} = \frac{1}{2\pi}\sqrt{k_{s_{in}}/m_s} = 95.4Hz.$$

A coupling between the cable network and the support in the out-of-plane direction is therefore expected given the value of $f_{s_{out}}$. Concerning the in-plane direction, the model prediction shows that the support is sufficiently rigid in this direction to neglect its amplitude.

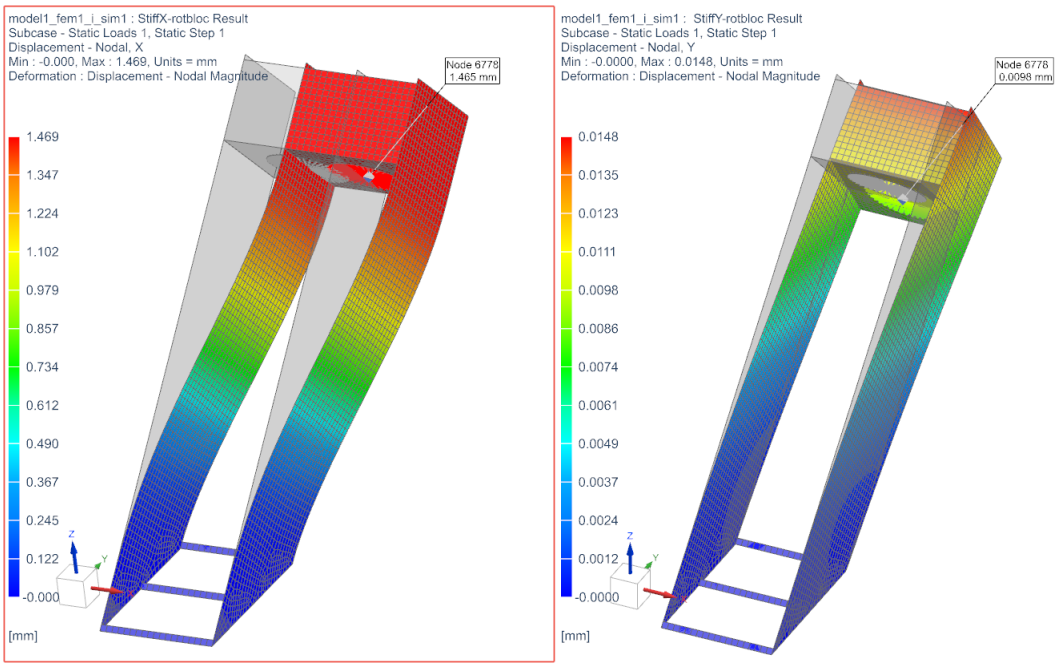

Figure 3.22: CAD model (Siemens NX) of the anchor support in the Milsaucy bridge and its static deformation in both directions due to an external force of 1 kN. (Developed by V2i company)

Experimental consideration

The flexibility of the supports in both directions can be further analysed by experimental measurements of the amplitude on these supports. To perform these, two accelerometers have been placed on both anchor supports measuring both the in-plane and out-of-plane vibrations. In this way, it is possible to directly compare the support amplitude with those of the sub-spans.

More precisely, the random excitations are studied by filtering the whole signal through a frequency acquisition window around the natural frequencies of the system. In this way, for each of the mono-harmonic filtered signal, an RMS value of the vibration amplitude can be obtained.

For the in-plane responses, the amplitudes of each of the sub-spans and of the corresponding support in the concerned direction are acquired. By applying the described

methodology, the estimation of the amplitudes of each modes participating to the global response can be obtained. These results are depicted in the upper part of Fig.(3.23), where the sub-figure in the left corresponds to the in-plane response of the first cable while the other in the right corresponds to the in-plane response of the second cable. The circle marker (O) and the plus marker (+) correspond respectively to the amplitude at the sensors positions of the upper span and of the lower span of the considered cable while the cross marker (X) depicts the amplitude of the support in the concerned direction. One may thus observe that the amplitude of the supports in the in-plane direction for each mode is always close to zero. These results enable therefore to conclude that the rigidity of the anchor supports in the plane of the cables network is sufficient to assume that the end sections of the cables are fixed in the corresponding transverse motion.
In addition to that, these figures bring additional information concerning the ratio of the amplitude at the sensor position between the upper and lower spans. In the in-plane response of the second cable, for instance, it seems that there exists an alternation between the eigenmodes where the highest amplitude is present in one of the sub-span of a given mode to be found in the next mode with the smaller amplitude. However, it can be noted that the third mode does not seem to participate to the response since no amplitude is observed at this frequency.

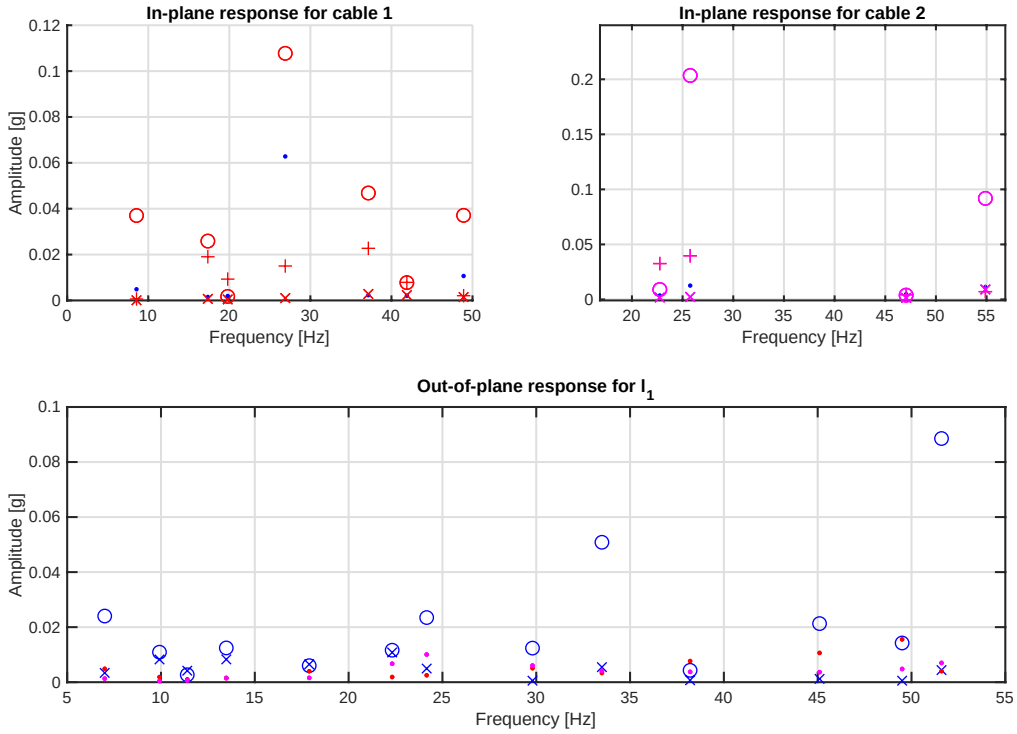

Figure 3.23: Amplitude of the cables and supports involved in the response for each mode. For the in-plane response, the markers (O) and (+) are respectively the amplitude at the accelerometer positions in the upper and lower span while the marker (X) is the support amplitude.

The support amplitude in the out-of-plane direction is also studied with the same approach. The amplitude of the sub-span l_1 (O marker) and its corresponding anchor support (X marker) in the out-of-plane direction are depicted in the lower part of Fig.(3.23) for the thirteen identified natural frequencies. As predicted by the model, the support presents large amplitudes, being sometimes even equal to the vibration amplitude of the cable. The stiffness of the support in the out-of-plane direction is therefore not sufficient to assume a perfectly fixed boundary condition at the cable ends. The out-of-plane model taking into account flexible anchor supports as previously described in section (2.3), will therefore be selected for the inverse method.
In order to validate the identification of the eigenfrequencies, the amplitude of vibration of the eigenmodes in a given plane of vibration can be compared with the amplitude in the perpendicular plane at these frequencies. It is thus possible to visualize directly if the natural frequency identified in a plane has not been confused with an eigenmode in the opposite plane. These amplitudes are marked with a dot in Fig.(3.23) for the colors corresponding to each response. It can effectively be seen that the resonant amplitudes are always greater than the amplitudes in the opposite plane. However, some exceptions can be identified for eigenmodes that do not participate much in the considered excitation.

Since the support amplitudes in the out-of-plane direction are comparable to the amplitude of the cables, both sensors located on these anchors should support the identification results obtained with the four other accelerometers. With the use of the random excitation realized on sub-span l_1 in the out-of-plane direction, it is possible to obtain the corresponding frequency responses of the anchor vibration by applying the methodology described at the beginning of this section. Fig.(3.24) allows noticing that the amplitude of vibration of the support is mainly observable at the low frequency. Moreover, it may be observed that the anchor supports are only excited through the cables since the frequency peaks coincide with the previously identified out-of-plane frequencies. The performed responses allow thus to support the identification results on the first natural frequencies of the out-of-plane problem, as discussed in section (3.2.3).

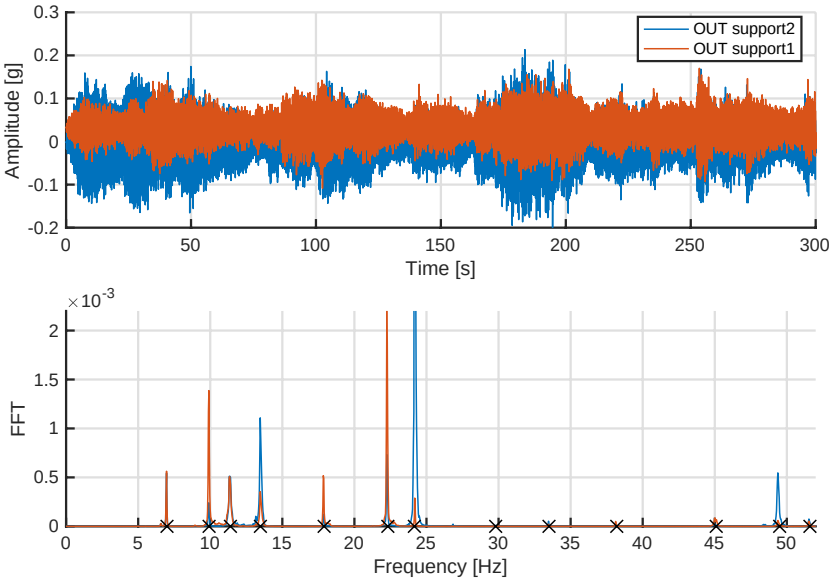

Figure 3.24: Response of the two anchor supports to random excitation in the out-of-plane direction and their corresponding FFT signals.

Chapter 4

Inverse problem analysis

Inverse problem analysis consists in finding characteristic parameters of a structure that best describe some observed indirect physical quantities. The vibration-based method is included in this indirect identification method by estimating these characteristic parameters through a set of observed natural frequencies. In the context of this thesis, the tensions, bending stiffness and boundary conditions of the cross cables network will be estimated with the vibration-based method through the FEM model and the experimental natural frequencies respectively presented in chapters 2 and 3. More precisely, optimization methods will be used to find the best properties of the cables by minimizing the error between the frequencies resulting from the FEM model and the experimental ones.
In a first step, the identification method will be introduced through the application of the reduced-scale model realized in the laboratory. This part will aim to validate the identification method. In a second part, the identification of the parameters will be realized for the cable network of the Milsaucy bridge.

4.1 Description of the optimization methods

Let's imagine the model $\mathbf{y}(\theta)$ as a function of the sought parameters θ related to the observations $\hat{\mathbf{y}}$ through the equality:

$$\hat{\mathbf{y}} = \mathbf{y}(\theta) + \mathbf{w} \tag{4.1}$$

, where w is the error assumed normally distributed with zero mean and constant variance σ^2. In this specific case, the function $y(\theta)$ corresponds to the eigenfrequencies returned by the FEM model with the bending stiffness EI and tensions T_i as parameters input θ while $\hat{\mathbf{y}}$ are the observed eigenfrequencies.
The principal objective is therefore to find the best properties EI and T_i that minimize the error ϵ.

4.1.1 Least square fitting

One approach used for this problem is the least square fitting, where the optimal parameters θ_{LS} are obtained by minimizing the error norm between the prediction model and the observations:

$$\theta_{LS} = argmin_{\theta}(\sum_{n}(\mathbf{y_n} - \hat{\mathbf{y}}_\mathbf{n})^2) \tag{4.2}$$

The function $\sum_n(\mathbf{y_n} - \hat{\mathbf{y}}_\mathbf{n})^2$ becomes thus the objective function to minimize. Since the model $\mathbf{y}(\theta)$ represents in most cases a nonlinear function of the parameters θ, an optimization algorithm needs to be implemented in order to find the optimal values θ_{LS}. One of the possibilities lies in optimization toolbox already implemented in `Matlab`. One of the candidate function is `fminsearch`, that find a local minimum of an unconstrained multivariable function. `fminsearch` uses the Nelder-Mead simplex algorithm as described in Lagarias et al.[5]. Basically, an iterative method is considered starting from an initial guess of the parameters to converge toward a local minimum using derivative-free method of the objective function. However, the algorithm is not guaranteed to converge to the global minimum which constitutes one of the main issue of the approach.
In order to obtain a first confidence interval on the obtained optimization parameters, it is possible to use the Laplace approximation. This consists in determining the behavior of the objective function at the considered minimum, by approximating locally the problem in a quadratic form of the variables. It is thus possible to obtain the covariance matrix of the model parameters $\mathbf{\Sigma}_\theta$ around the minimum by computing the curvature matrix as

$$\mathbf{H} = \frac{\partial^2}{\partial\theta^2}\sum_{i=1}^{n}\frac{\left(\hat{y}_i - \mathrm{y}_i(\theta_{LS})\right)^2}{2\sigma_w^2} \tag{4.3}$$

, where σ_w represent the final standard deviation between the model and the observations

$$\sigma_w^2 = \frac{1}{n}\sum_{i=1}^{n}\left(\hat{y}_i - \mathrm{y}_i(\theta_{LS})\right)^2. \tag{4.4}$$

The covariance of the model parameters is then simply given by the inverse of the curvature matrix. The variance of each parameters are represented in the diagonal terms of $\mathbf{\Sigma}_\theta$ while the covariance between them are included in the off-diagonal terms. A first approximation of a Gaussian PDF can finally be deduced for each parameter with mean value corresponding to the optimal parameters θ_{LS} for their associated computed variance.

4.1.2 Maximum likelihood approach

Probabilistic method can also be implemented in order to find the most probable values of the model parameters. In this approach, a complete joint probability density function is obtained indicating how much confidence one can have in the model parameters instead of having only a best value of these parameters.
This PDF is obtained from the Bayes' theorem of conditional probabilities:

$$p(\theta|\hat{\mathbf{y}}) = \frac{p(\hat{\mathbf{y}}|\theta)p(\theta)}{p(\hat{\mathbf{y}})} \sim p(\hat{\mathbf{y}}|\theta)p(\theta). \tag{4.5}$$

The likelihood $p(\hat{\mathbf{y}}|\theta)$ indicates the probability to observed $\hat{\mathbf{y}}$ for a model with parameters θ. The prior distribution of the model parameters $p(\theta)$ corresponds to some priori information that could be obtained without any knowledge of the experimental observations. If it is assumed that anything is known from this prior distribution, a so-called uninformative prior can be used, i.e. $p(\theta) = cst$.
Consequently, the maximum likelihood estimator of the model parameters consists in maximizing the likelihood, or in general case, the log-likelihood

$$\mathcal{L}(\theta) = \log p(\hat{\mathbf{y}}|\theta). \tag{4.6}$$

The model parameters maximizing this likelihood function are therefore given by

$$\theta_{\mathrm{ML}} = \arg\max_{\theta} \mathcal{L}(\theta). \tag{4.7}$$

However, the distribution $p(\hat{\mathbf{y}}|\theta)$ is difficult to estimate in practise. That's the reason why some approximate method to counter that problem can be used such as those of the Monte Carlo Markov Chain (MCMC) family, which includes the Metropolis-Hastings algorithm.
As described by Yildirim [12], the Metropolis-Hastings (MH) algorithm simulates samples from a probability distribution by making use of the full joint density function for each of the variables of interest. To obtain the full details of a generic MH algorithm, refer to Yildirim [12].
Practically, the generated samples depend on an initial value considered as an input in the algorithm. A burn-in zone in the iteration is therefore present corresponding to the first iterations where the algorithm is not yet stabilized. This zone needs thus to be carefully identified to discard it in the estimation of the prior distribution of each parameter. The latter has to be calibrated depending on the complexity of the model and the number of parameters to identify. The algorithm continues then to generate samples of the unknown parameters in a predefined interval. Once the maximum established number of iterations

realized, the prior distribution of the parameters can be approximated by computing histograms. Mean values and standard deviations can then be deduced for each model parameter. The MH algorithm provides thus a range of possible values for each parameter with their associated likelihood to be observed directly through the histogram of the corresponding iterations sample.

4.2 Application

In the following application, the methods of optimization resulting from toolbox of `Matlab` and the Metropolis-Hastings algorithm are applied with the collected data of the reduced-scale model and the Milsaucy bridge.
As introduction to both methods, the tension and the bending stiffness are estimated through the natural frequencies obtained in laboratory for the single steel cable. Through this first application, an estimated percentage of tension loss through the static torque resistance of the pulley will be defined. The full reduced scale model is then analyzed to validate the inverse approach applied to a crossed cable network.
Finally, the inverse method is applied with the aim of estimating tensions in the selected two cross cables network of the Milsaucy bridge. The tensions estimated through the in-plane model are then compared to the ones of the out-of-plane model to see if there is indeed an actual correlation between them. The inverse approach will also provide an estimate of the secondary parameters of the problem being the bending stiffness of the cables and the flexibility conditions at the anchor supports.

4.2.1 Identification in single cable model

The inverse approach is introduced here with the use of the experimental natural frequencies of the simple cable realized in the laboratory. At first, the function `fminsearch` from the optimization toolbox of `Matlab` is used to obtain the optimal tension and bending stiffness minimizing the error norm between the frequencies of the FEM model and the observed ones. Let's apply the optimization function for the seventeen identified natural frequencies of the single cable configuration with an applied tension of 10kg (cfr. section(3.1.1). These experimental frequencies are depicted in Fig.(4.1) with the ones resulting from the estimated optimization parameters of the model. One may observe that the optimization function has indeed found an interesting match between those two sets of frequencies. The resulting identified tension corresponds to 90.82 N for an applied mass in the set-up of 98.16 N, corresponding thus to a relative error between them of -7.4%. However, it is worth noting that the presence of the pulley between the attached mass and the studied cable reduced the internal tension through a static torque resistance. A small difference between them is therefore expected. To validate this percentage of tension losses in the pulley, the inverse method will be applied for the two other tests to see if these values stay in the same order of magnitude.
Concerning the bending stiffness estimation, the algorithm returns a value of 0.55 mN/m which is, as expected, negligible.

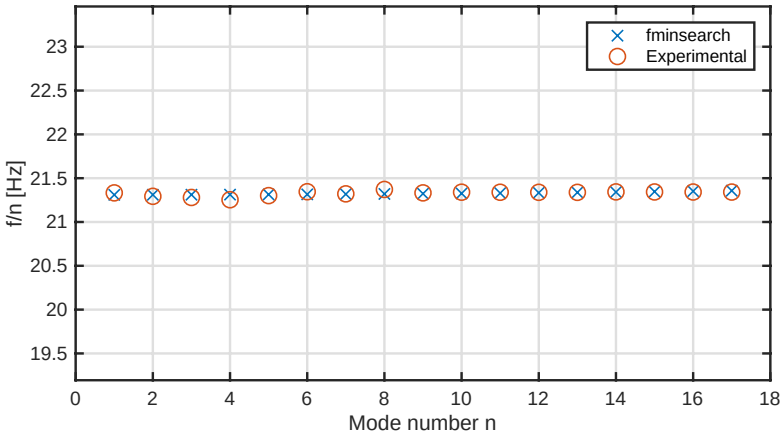

Figure 4.1: Comparison between the experimental natural frequencies and the ones obtained through the model with the optimization parameters resulting from `fminsearch` for the single cable.

By computing the curvature matrix of the objective function locally at the optimization point, a first estimation of the variance of each parameters can be obtained as described in the previous section(4.1.1). A first picture of a Gaussian PDF can finally be represented for each of the parameters (Fig.4.2). A 2σ confidence interval can also be depicted in both PDF in order to see how much confidence one can have on the obtained parameters. It seems thus that bending stiffness parameter is difficult to identify since its confidence interval is large comparing to its mean value. This observation is once again in agreement with previous results, showing an insignificant influence of bending stiffness on the observed frequencies. It is worth noting that the a small part of this PDF distribution is located in the negative part of the bending stiffness which must obviously be rejected. This constitutes an additional issues in the Laplace approximation which does not take into account any physical interval in which the parameter can lie. The Laplace approximation brings however excellent result for the tension estimation given its low variance.

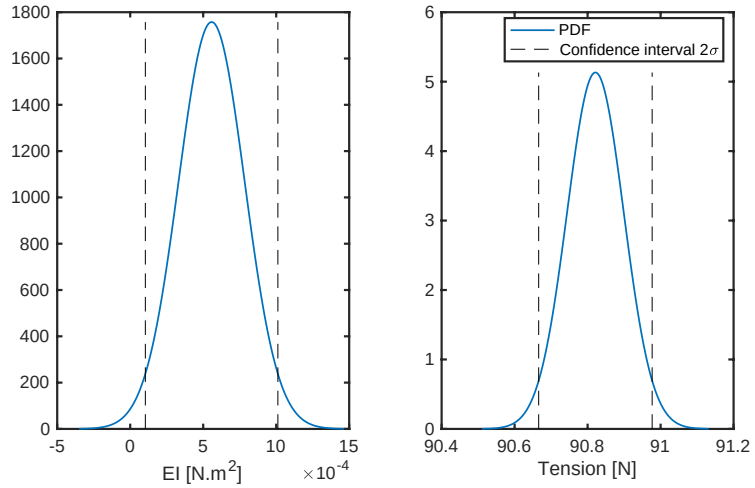

Figure 4.2: Laplace approximation of Gaussian PDF of the optimization parameters EI and T resulting from `fminsearch` for the single cable model.

The estimation of tension and bending stiffness can be further analyzed by computing a prior distribution for each of these parameters through the Metropolis-Hasting algorithm. The initial values for tension and bending stiffness are respectively set to 100 N and 10 mN.m^2. The respective upper and lower bound values of the tension are defined as one-tenth and ten times its initial value while the inspectable interval of the bending stiffness is set to one thousandth and a thousand times its initial value. The whole set of samples obtained after 1500 iterations for both parameters are depicted in Fig.(4.3). After 500 iterations, one can see that the samples converge towards their most likely values. The first transient zone of the samples, called the burn-in zone, needs to be discarded for both samples.

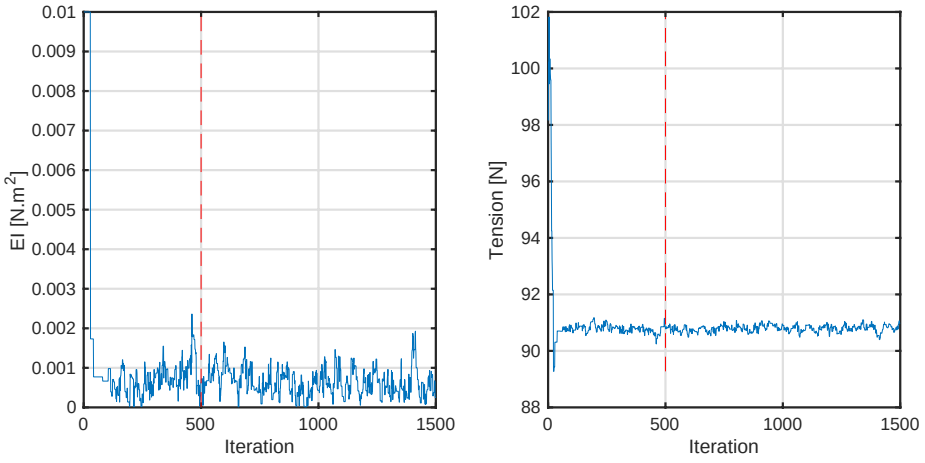

Figure 4.3: Tension and bending stiffness samples of the MH algorithm along the iterations for the single cable model.

The stationary part of the samples can then be analyzed to build histograms of the unknown parameters (Fig.4.4), from which can be deduced the mean values and the

variance σ of the parameters. As realized in the Laplace approximation, a confidence interval can be defined with a deviation from the mean value of 2σ. The histogram related to the tension is indeed similar to a Gaussian distribution while the EI probability distribution is more related to a right-skewed normal one constrained by its lower bound near zero.

Although offering only local information of the problem, it can be seen that the Laplace approximation brings interesting results from a stochastic point of view given the rather accurate estimation of the mean values and variances compared to the MH algorithm.

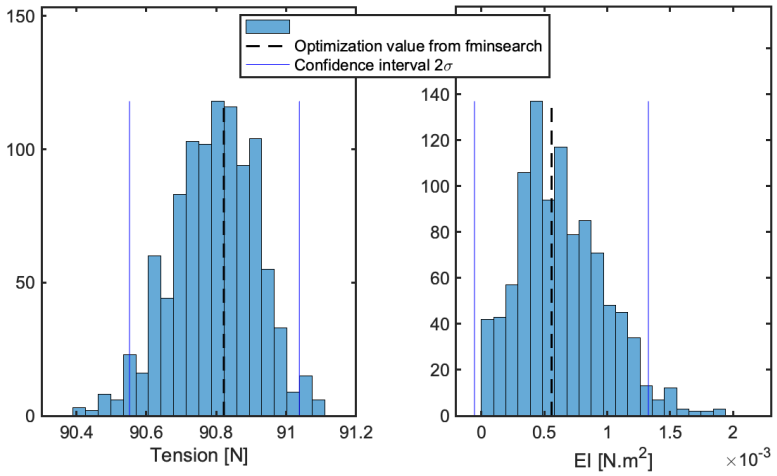

Figure 4.4: Histograms of the tension and the bending stiffness of the single cable model deduced from the steady part of the MH samples.

The previous complete analysis is then carried out for the other two configurations of the single steel cable to see if the same conclusions can be drawn. The final estimate of the tensions and their respective confidence intervals for both methods are given in Table(4.1) for applied tensions of 19.8 N and 39.3 N. It can be observed that there is an almost perfect match in the estimation of the mean values between the two methods. A very narrow confidence interval is observed in all three configurations, allowing thus to assign high confidence to the estimated tensions. Eventually, a percentage of tension loss assigned to the torque resistance in the pulley is evaluated and depicted in bracket from the lowest possible applied tension to the highest possible one in the set-up. The corresponding values allow thus to conclude that these tension losses stay approximately constant for each applied tension configuration with an average round value fixed to 7%. For the rest of the inverse method applied to the reduced-scale model, the reference tension will be thus constantly evaluated thanks to this relation.

An estimation of the bending stiffness of the cable is however not relevant in this case, as this one has a negligible influence on the result. It can be seen that its estimation is more related to measurement errors in the experimental identification of the natural frequencies of the system rather than a real physical value. One can therefore conclude

that the configuration of the single cable used returns a zero value of this stiffness.

T_{app}	$\mathrm{T}_{fminsearch}(\epsilon_T)$	$\mathrm{CI}_{fminsearch}$	$\mathrm{T}_{MH}(\epsilon_T)$	CI_{MH}
19.8	18.3 (-7.6%)	[18.18 ; 18.42]	18.25 (-7.8%)	[18.05 ; 18.45]
39.3	36.6 (-6.9%)	[36.56 ; 36.71]	36.58 (-6.9%)	[36.35 ; 36.8]
98.16	90.82 (-7.4%)	[90.67 ; 90.98]	90.8 (-7.4%)	[90.53 ; 91.1]

Table 4.1: Overview of the estimated tension for the single cable model.

4.2.2 Application to the in-plane reduced-scale model

The method of identifying the cable network is now introduced through the laboratory model. The tension in one of the two cables can be evaluated thanks to the previously identified in-plane natural frequencies. Moreover, it is found that the stiffness effect in a cable increases when the actual length of the cable decreases. It is therefore expected that bending stiffness will have a greater influence on this problem than in the case of the cable alone. This one will try to be more precisely identified in this problem. For recall, the physical model relying on the in-plane experimental set-up corresponds to the single cable simply supported at both ends with intermediate support taking into account the crossing restraint (cfr.2.2).

As presented in the introduction before, the use of the function `fmincon` is first applied to obtain the global minimum of the objective function corresponding to the sought parameters. Let's take the set-up of the first configuration corresponding to the smallest applied tension, that is 4kg (cfr.2.2). The reference tension is fixed to this value reduced by the relative 7% losses previously identified. Fig.(4.5) shows the similarity between the experimental frequencies and those resulting from the model after convergence of the identification method.

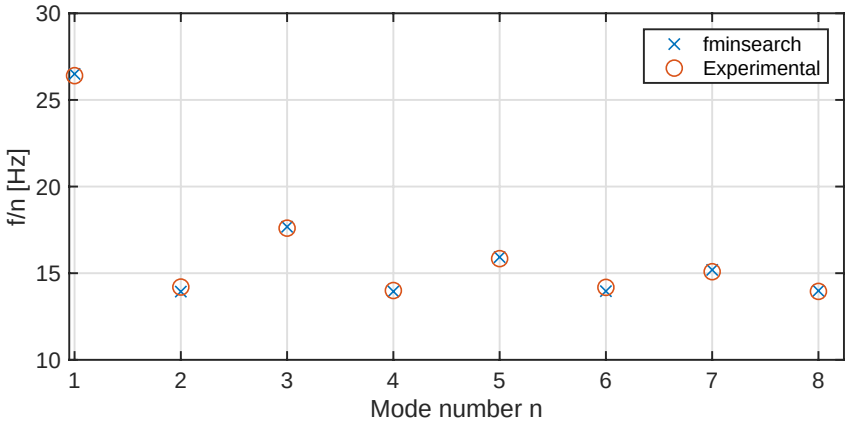

Figure 4.5: Comparison between the experimental natural frequencies and the ones obtained through the model with the optimization parameters resulting from `fminsearch` for the in-plane problem.

It may be observed that both sets of frequencies are indeed very close allowing us to notice that a minimum of the objective function has been effectively reached. The resulting optimal tension corresponds to 36.65 N for a reference value of 36.55 N which seems to be an interesting optimum. However, a relevant conclusion can only be drawn on a value if a confidence interval can be assigned to it. By calculating the curvature matrix of the objective function considered as locally quadratic at the minimum found, a first approximation of the variance is obtained. A 2σ confidence interval centered at the estimated tension can then be represented through a Gaussian probability distribution, as depicted in the right Fig.(4.6).
By realizing the same procedure for the bending stiffness parameter, the optimal found value is 1.6 mN.m^2 for a variance of 3.7 mN.m^2. A Gaussian PDF representation of this parameter, therefore, gives a distribution approximately centered around zero with a non-negligible part of observing a negative value (Fig.4.6). This, of course, makes no physical sense so it is possible to conclude once again that the identification method does not allow to identify this parameter on the first experimental in-plane natural frequencies for the concerned cable.

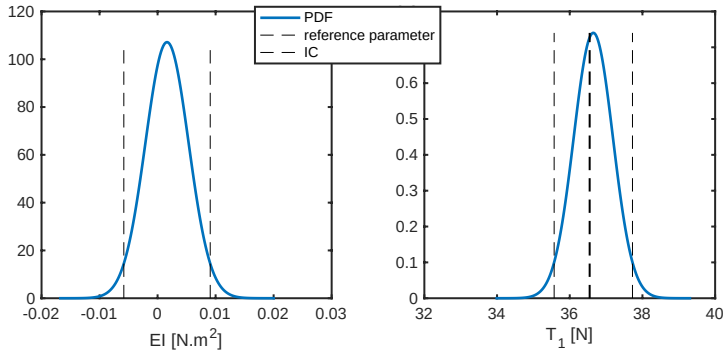

Figure 4.6: Laplace approximation of Gaussian PDF of the optimization parameters EI and T resulting from `fminsearch` for the in-plane problem.

The Metropolis-Hasting algorithm is then considered for comparison. The initial values of tension and bending stiffness are arbitrarily set to 20 N and 0.01 N.m^2 while their upper and lower bounds are fixed in a similar way to the single cable model previously described. The set of samples obtained after 2000 iterations are depicted in Fig.(4.7) with an identified burn-in zone for the first 500 iterations. Histograms of the stationary MH samples are then deduced, from which a 2σ confidence interval around the most observed value is computed for each parameter (Fig.4.8). The probability distribution related to the bending stiffness shows this time a decreasing exponential behavior supporting the fact that the most explored value is zero. As with the single cable, the distribution related to the tension is similar to a Gaussian one with the presence of some outliers. The algorithm seems to provide good estimations of the tension parameter given the proximity between the mean value and the reference tension. Unfortunately, the inverse approach applied

to the bending rigidity brings us to the same conclusion as before. Therefore, only the identification results linked to the tension will be presented for the rest of the reduced-scale model application while keeping the bending stiffness as an identification parameter in the problem.

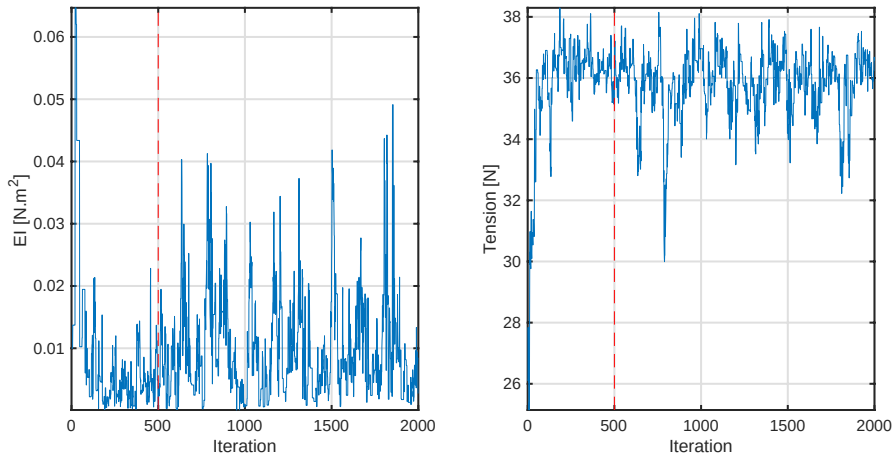

Figure 4.7: Tension and bending stiffness samples of the MH algorithm along the iterations for the single cable model.

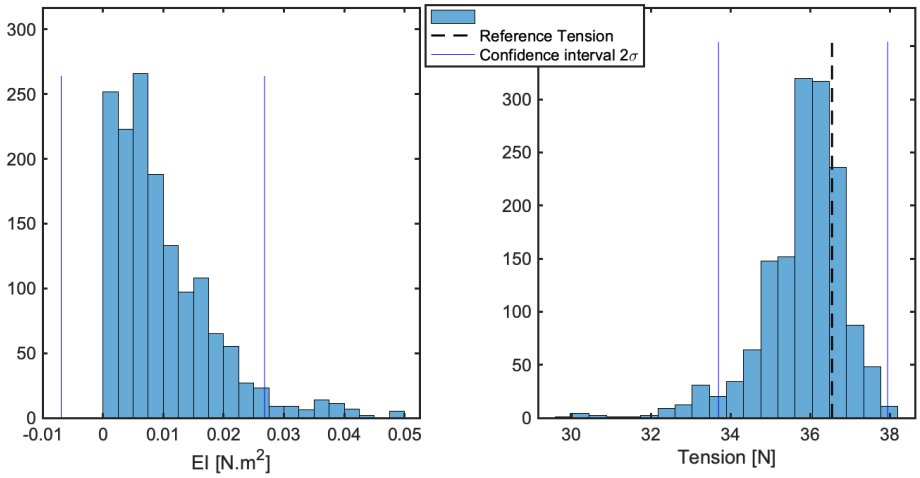

Figure 4.8: Histograms of the tension and the bending stiffness of the single cable model deduced from the steady part of the MH samples.

The full optimization procedure of the inverse method is then conducted for the other five configurations of the in-plane reduced scale model. An overview of the tension estimation for the six configurations is depicted in Fig.(4.9). The results of the MH algorithm are presented in the form of Boxplot, while the optimization parameters resulting from the function `fmincon` are depicted with the green star marker between its corresponding 2σ confidence interval with the green dotted line. The three first results correspond to the first geometrical configuration, while the three others refer to the second one.

It can be seen that the reference tension is always between the upper and lower limits of the boxplot so that a fairly good estimate of the sought parameter is achieved. The optimal tension obtained through the `fminsearch` function also shows satisfactory results, the latter being generally in the boxplot or close to it. However, one can see that the estimated tension is always underestimated, and this is specifically for the MH algorithm. The in-plane model seems thus to be a bit stiffer than reality.
It is also possible to visualize that the local approximation of the confidence interval assigned to the parameter is quite close to the Bayesian result. Therefore, when it is necessary to quickly evaluate the confidence interval of an optimization parameter, the Laplace approximation becomes an interesting method for the concerned problem.

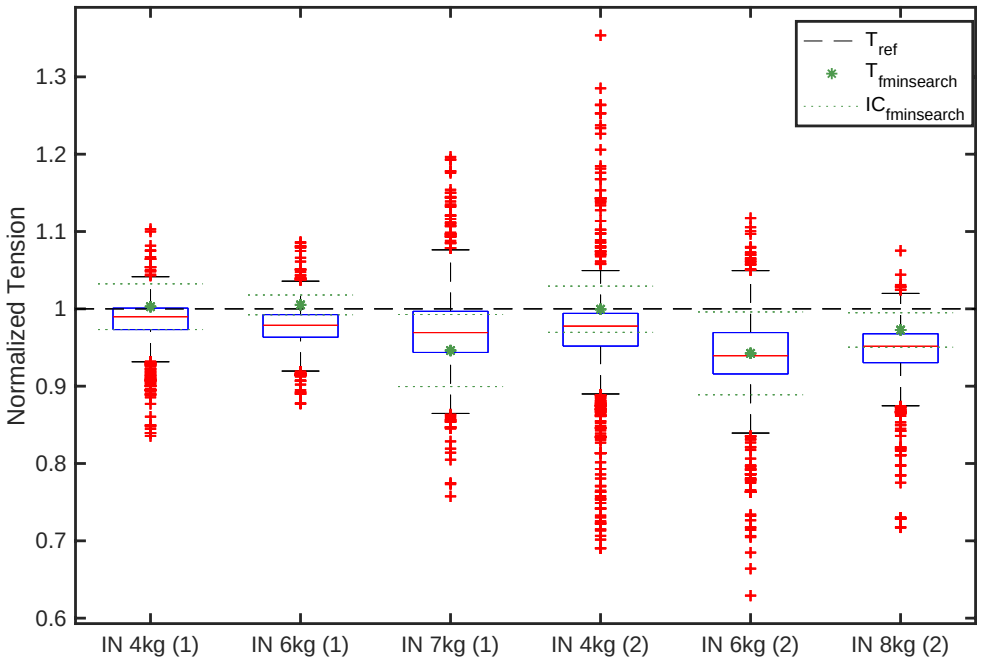

Figure 4.9: Overview of the estimated tensions for the six configurations of the in-plane reduced scale model.

4.2.3 Application to the out-of-plane reduced scale model

Let's apply now the inverse estimation to the out-of-plane problem of the considered reduced scale model. To avoid redundancy, just the final results are presented here. It should be noted however that the conclusions drawn from the out-of-plane problem lead to the same observations; namely, among other things, that no improvement is present in the identification of the bending stiffness. Fig.(4.10) and (4.11) show the final results of the out-of-plane problem in the same form as the in-plane problem, where the annotation OUT$a_b(c)$ is translated as the out-of-plane problem of the geometrical configuration c for applied tensions in the first and second cable respectively equal to a kg and b kg.

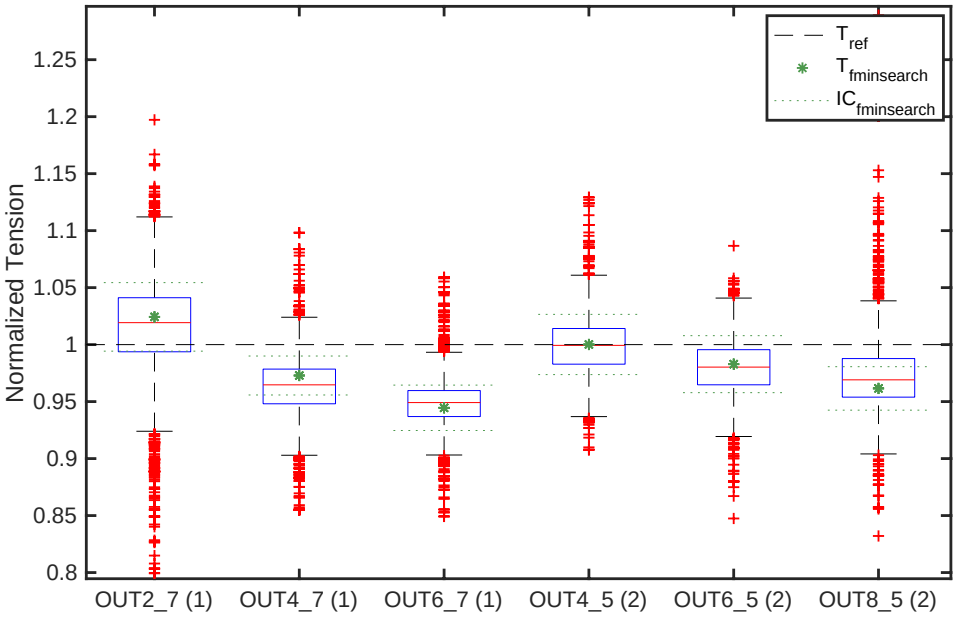

Figure 4.10: Overview of the estimated tensions of the **first** cable for the six configurations of the out-of-plane reduced scale model.

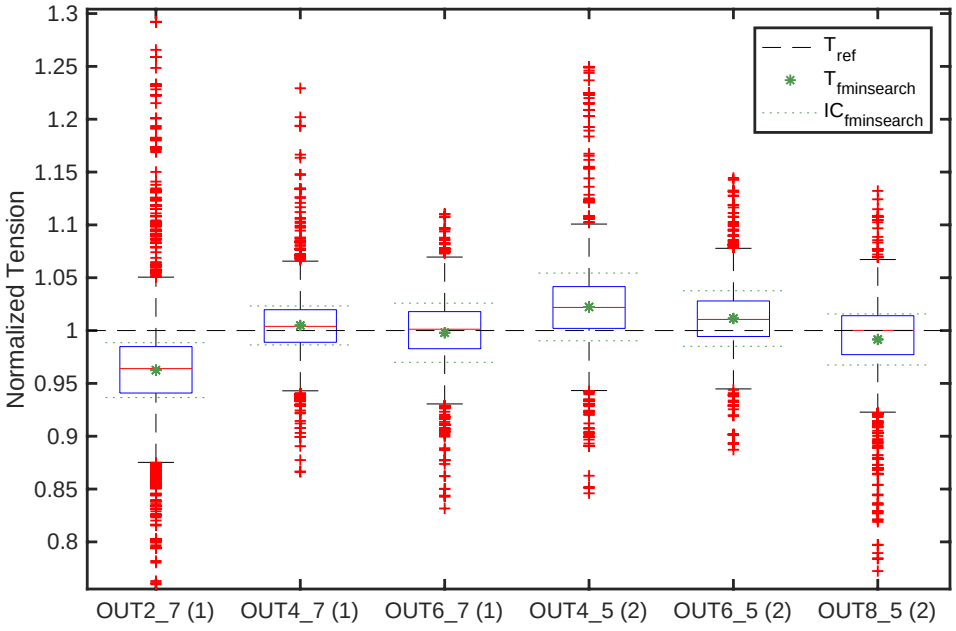

Figure 4.11: Overview of the estimated tensions of the **second** cable for the six configurations of the out-of-plane reduced scale model.

4.2.4 Milsaucy Bridge application

The inverse analysis performed on the reduced-scale model have shown that it was impossible to identify the bending stiffness of the concerned cable, this one being close to zero. Moreover, the considered boundary conditions could be assimilated to idealized supports, which did not allow any discussion on the influence of the identification approach with flexible supports consideration. However, the method allows in these conditions to validate the identification of the tensions being previously known through the two proposed methods. The application to a real case allows to verify that the method of identification of tensions in a network of crossed-cables having a non negligible bending stiffness with flexible supports is feasible with the proposed approach.

In-plane identification

The experimental test performed on the stays 1 and 2 of the Milsaucy Bridge presented in Chapter 3 has allowed the identification of the first seven natural frequencies in the in-plane problem of cable 1, and the first four frequencies in cable 2. The vibration amplitude at the supports in this direction has led to the conclusion that the rigidity of the anchors is sufficient to consider them fixed. The physical model relying on the observations corresponds to the simple supported tensioned beam where the crossing point is considered as a simple intermediate support, as discussed in Chapter 2. In the in-plane direction, the identification problem relies thus only on the estimation of the tension and the bending stiffness on the concerned stay. To obtain a complete knowledge of the cable network, the identification approach must therefore be applied to each cable. In this part, tension and bending stiffness values are estimated in the two cables presented simultaneously to obtain a complete knowledge of the cable network parameters. Since only four in-plane frequencies have been identified in cable 2 compared to seven in cable 1, it is expected to obtain higher confidence in the estimated parameters of the first cable due to the higher a priori information on the problem. By application of the optimization function `fmincon`, the first couple of tension and stiffness in each cable is obtained, and presented in Table (4.2) with their respective 2σ confidence intervals obtained through a Laplace approximation. These values will be further discussed through comparison with the Bayesian results. Fig.(4.12) shows the result of the final convergence between the observed frequencies and those of the model with the estimated parameters.

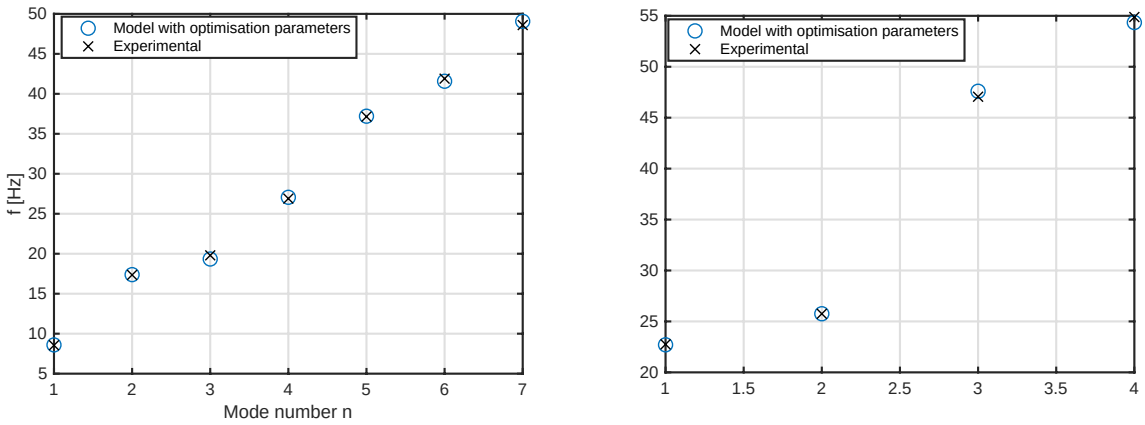

Figure 4.12: Comparison between the experimental natural frequencies and the ones obtained through the model with the optimization parameters resulting from `fminsearch` for the in-plane problem of the Milsaucy bridge.

	T[kN]	IC_T [kN]	EI [kN.m^2]	$IC_{EI}[kN.m^2]$
Cable 1	1221.2	[1186.2 1256.2]	230.3	[192.3 268.3]
Cable 2	1756.7	[1698.9 1814.5]	185.2	[134.5 235.8]

Table 4.2: Estimated tension and bending stiffness values from the in-plane problem of the Milsaucy bridge through `fmincon`.

The Bayesian approach is then considered through the MH algorithm to broaden the confidence that can be attributed to the results. The initial values of tension and bending stiffness are arbitrarily set to 1000 kN and 200 kN.m^2 while their upper and lower bound are fixed once again to one-tenth and ten times their initial values. The set of samples obtained after 4000 iterations are depicted in Fig.(4.13) simultaneously for both cables with an identified burn-in zone corresponding to the first 1000 iterations. The corresponding histograms are then deduced and represented in the lower part of the same figure. From this figure, one can see that the parameters related to the model of the second cable scan a much larger domain than those of the first cable. A visualization of this effect is directly reflected in the width of the associated histogram distribution. This is, as expected, directly related to the weaker prior information of the second cable. Larger confidence is therefore attribute to the results of the first cable compared to the second one.

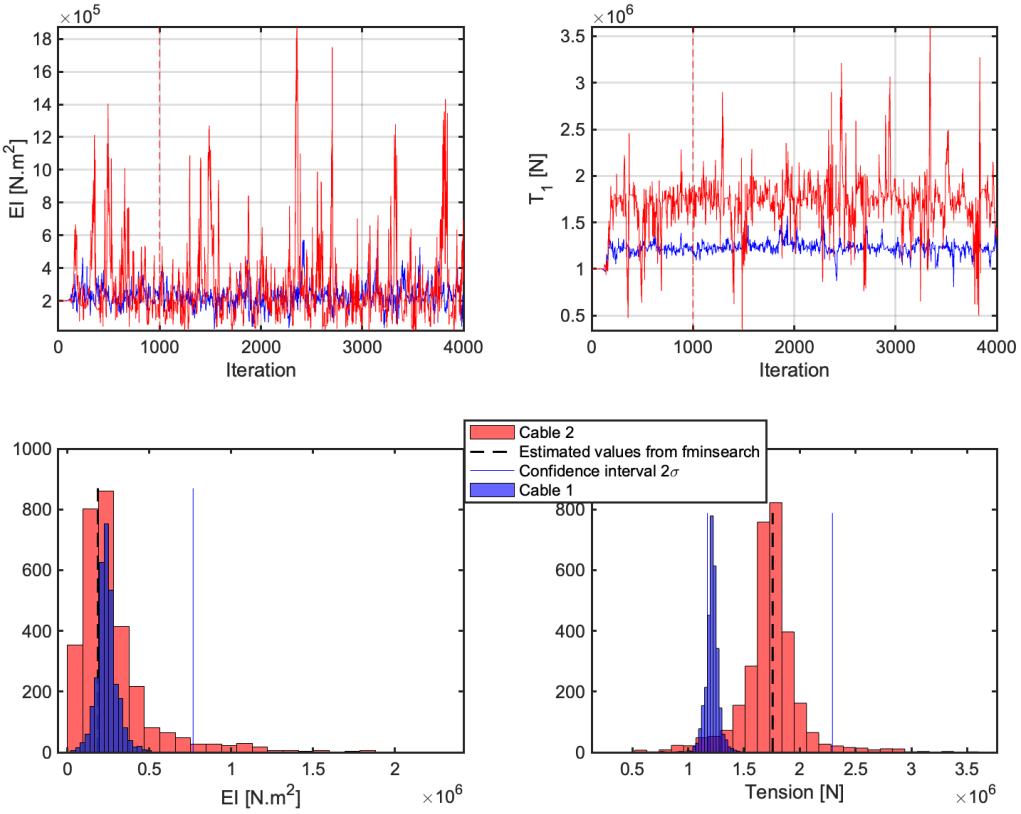

Figure 4.13: Tension and bending stiffness samples of the MH algorithm along the iterations and their corresponding histograms for the in-plane problem of the Milsaucy bridge.

The statistical analysis of the results can also be studied by considering only the most encountered values in the samples through Boxplot. Fig.(4.14) and (4.15) present these results with those of the Table (4.2) from `fminsearch`. An important observation is thus directly visualized in these two figures, namely that the estimation of the parameter through the `fminsearch` function returns a value that coincides with the most probable value of the MH algorithm. In addition, the results show that the confidence interval estimate obtained by the Laplace approximation to the minimum objective function gives an excellent estimate of the confidence attributable to the optimal parameters. One reason for this great match lies in the fact that the optimization function can be effectively seen as quadratic at the absolute minimum given the bell-shaped histograms.

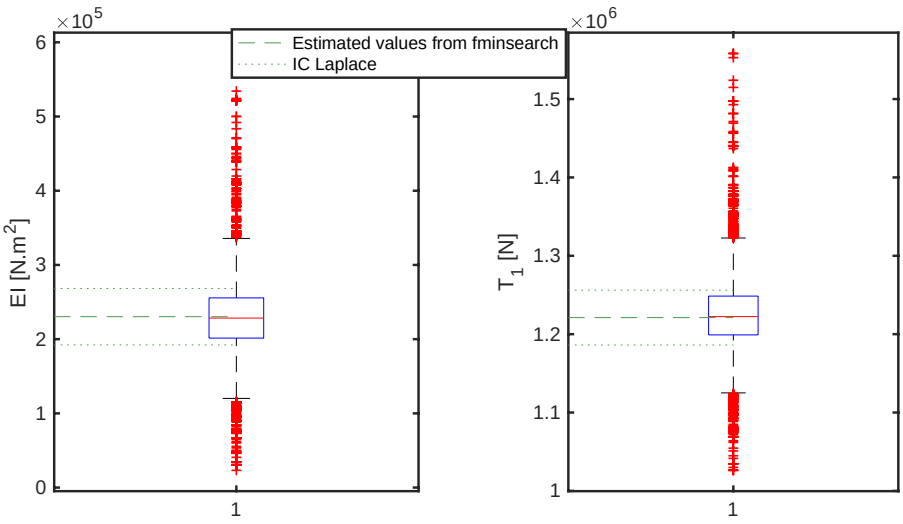

Figure 4.14: Boxplot of the estimated parameters of the **first** cable from the MH samples of the in-plane problem.

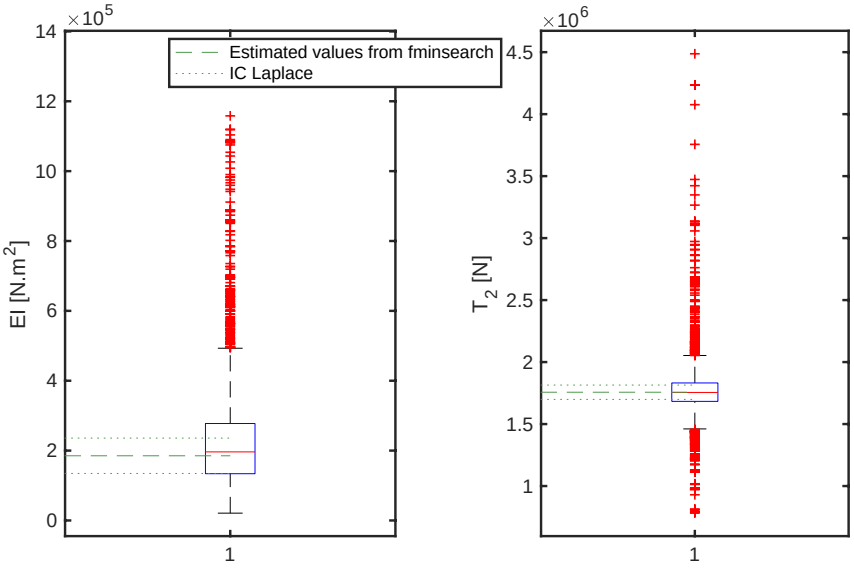

Figure 4.15: Boxplot of the estimated parameters of the **second** cable from the MH samples of the in-plane problem.

Out-of-plane identification

The experimental measurements carried on the cable 1 and 2 of the Milsaucy bridge in the out-of-plane direction have shown that non-negligible amplitude at the anchor support did not allow the assumption of a perfectly fixed anchor support. This led to the introduction of a translational stiffness and mass for the degrees of freedom previously assumed to be blocked. These two parameters are added to the unknowns of the out-of-plane identification problem.
In this part, new values of bending stiffness, and tensions in the two cables will be obtained. These values will then be compared to the results of the in-plane problem in order to validate the whole inverse approach, and to note potential concerns. The flexibility properties of the support will also be estimated; namely, its equivalent rigidity and mass.

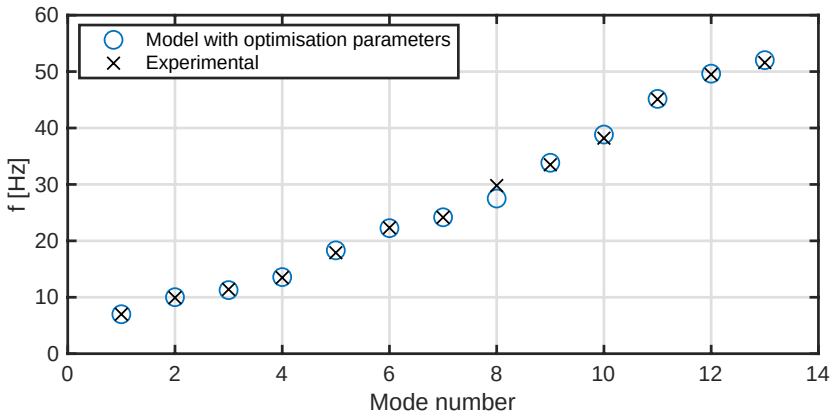

Figure 4.16: Comparison between the experimental natural frequencies and the ones resulting from the optimization procedure through `fminsearch` for the out-of-plane problem of the Milsaucy bridge.

As always, a first approximation of the set of unknown parameters can be obtained through the function `fmincon`. The first thirteen out-of-plane identified eigenfrequencies can then be visualised in Fig.(4.16) with the ones resulting from the optimization procedure. From these optimisation parameters, it is possible, as always, to obtain a Gaussian distribution of the parameters through the Laplace approximation as depicted in Fig.(4.17) and (4.18). It was found during the in-plane identification problem that these confidence intervals offered very satisfactory results, these ones being almost similar to the quartiles resulting from the samples of the MH algorithm. Using these previous results, it is possible to obtain a first comparison of the tension estimates in the two cables, as well as a third estimate of the bending stiffness. These results are thus presented all together with the use of the Gaussian approximation in Fig.(4.17). One may observe that the inverse approach of the out-of-plane provides estimates with much larger confidence intervals as the ones resulting from the in-plane problem. Less confidence is therefore given to the parameter estimated through the out-of-plane model. Concerning the estimates of tension, it can

be observed that the credible intervals of each parameters resulting from the in-plane are always include in the ones of the out-of-plane problem, strengthening the credibility of the inverse method to identify these tensions. However, the estimation of the bending stiffness of cables seems to be more difficult to obtain. A good average estimate of this value can however be obtained thanks to the in-plane results having a fairly narrow and close distribution.

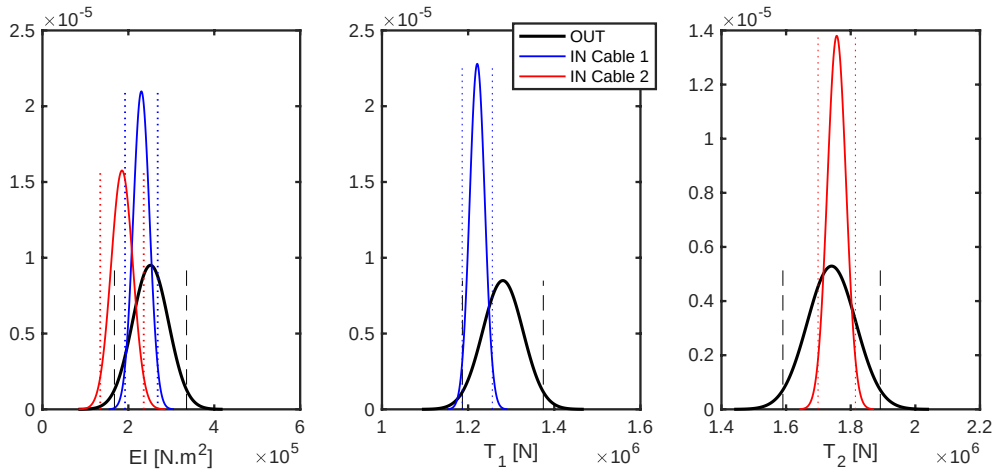

Figure 4.17: Laplace approximation of Gaussian PDF of the optimization parameters EI, T_1 and T_2 resulting from `fminsearch`

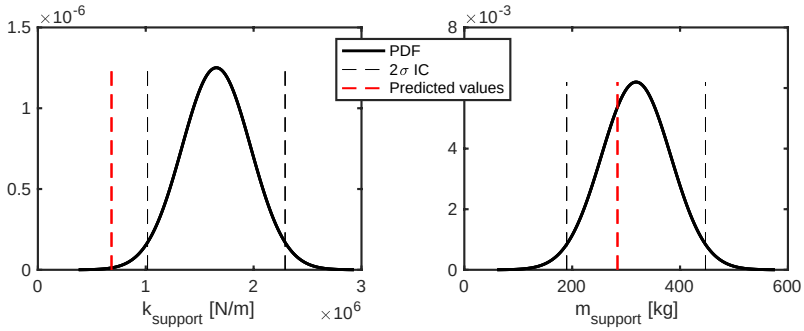

Figure 4.18: Laplace approximation of Gaussian PDF of the parameter linked to the flexibility of the anchor support in the out-of-plane direction.

Concerning the estimates of the flexibility properties of the anchor supports, their Gaussian distribution appears to be quite broad, so that it is also difficult to obtain an accurate estimate of them. It can also be seen that the predicted values obtained thanks to the CAD model, described in section (3.2), fall within the credible interval only for the estimation of the mass value. Unfortunately, the MH algorithm applied to the concerned out-of-plane model turns out to be not applicable. Indeed, the optimization are not able to find a steady convergence, in such a way that the samples of all the parameters varies constantly between their upper and lower limits. Consequently, any result coming from the MH algorithm will be presented for the out-of-plane application.

Therefore, the out-of-plane identification proves to be useful by a global estimation of the properties of the whole cable network in one single step. However, it provides credible intervals that are quite broad in such a way that a precise estimation of these parameters stays difficult.

Chapter 5

Conclusion

In this thesis, the dynamic behavior of a two crossed-cable network has been analyzed for the implementation of an identification procedure that aims at defining cable properties from a given set of observed natural frequencies. First, the direct analysis of the proposed structural scheme has been developed through a FEM whose results have been compared to some analytical outcomes. Then, some experimental measurements have been carried out through a reduced scale model of the structural network to acquire a first set of eigenfrequencies for previously known tensions. Inverse analysis based on optimization methods has then been introduced through these observed eigenfrequencies as a validation purpose for the identification of tensions. Eventually, the validation of the identification method has been achieved through experimental natural frequencies on a real cable network, leading to the consideration of flexible supports.
Specifically, the key results presented in this studies highlight that:

- Bending stiffness brings additional degrees of connection between the transverse vibration of the spans. When the latter is included in the model, the natural frequencies follow a quadratic evolution in each of the vibration planes in contrast with a linear evolution when the parameter is neglected.

- Flexible supports have to be included in the model as soon as their characteristic frequencies are of the some order of magnitude than the natural frequencies of the cable network.

- The use of scaled-down models allows the validation of the identification approach by prior knowledge of the system parameters. However, these configurations are often constrained in terms of space and the choice of suitable boundary conditions. Consequently, these do not always provide the same conditions as those encountered in practice.

- In the identification approach, the Bayesian algorithm turns out to be a powerful tool to get overall ranges of values in which there is a high probability that the

real values fall. The use of the function `fminsearch` from the optimization toolbox of `Matlab` has also proved to be effective in the identification strategy, being in most cases very close to the most probable values of the first algorithm. Moreover, it was found that the Laplace approximation delivers an accurate credible interval in the neighborhood of the identified parameters, allowing to provide a complete identification approach with the use of `fminsearch`.

- The in-plane inverse method turns out to be more accurate in the identification of its governing parameters compared to the out-of-plane identification strategy. However, the out-of-plane identification proves to be useful for a global estimation of the properties of the whole cable network in one single step.

Future works

Several improvement perspectives arise from this work.
First of all, the construction of a more complex reduced-scale model taken would be interesting. Indeed, the effects of flexible support would be deeper understood by considering them directly on a scaled-down model. In consequence, this would allow a potential improvement of the physical model, resulting in a more accurate estimation of the properties when applied in a real case.
Finally, tension monitoring can only be realized if a completely autonomous algorithm is performed. It could be thus interesting to develop software involving all the previous results to obtain a continuous health status of civil engineering structure.

Bibliography

[1] R.Kobayashi A. Furukawa, S.Yamada. Tension estimation methods for two cables connected by an intersection clamp using natural frequencies. *Journal of Civil Structural Health Monitoring*, 2021.

[2] H. Tabatabai A. Mehrabi. Unified finite difference formulation for free vibration of cables. *J. Struct. Eng.*, 1998.

[3] C. Gentile F. Benedettini. Operational modal testing and fe model tuning of a cable-stayed bridge. *Eng. Struct.*, 2011.

[4] H. M. Irvine and T. K. Caughey. The linear theory of free vibrations of a suspended cable. *Royal Society*, 1974.

[5] Margaret H. Wright Jeffrey C. Lagarias†, James A. Reeds and Paul E. Wright. Convergence properties of the nelder–mead simplex method in low dimensions. *SIAM Journal on Optimization*, 2014.

[6] C. Prato M. Ceballos. Determination of the axial force on stay cables accounting for their bending stiffness and rotational end restraints by free vibration tests. *J. Sound. Vib*, 2008.

[7] E.Verstraelen P.Toussaint V.Denoël M.Geuzaine, F.Foti. Development of a general monitoring program for bridge stays and hangers in wallonia, belgium. .

[8] V.Denoël M.Geuzaine, F.Foti. On the identification of axial force in stay cables anchored to flexible supports. .

[9] Daniel J. Rixen Michel Géradin. *Mechanical vibrations theory and application to structural dynamics*. Wiley, 3 edition, 2015.

[10] N-M.Pereira. Vibration of small sag cables equiped with viscous dampers. *Instituto Superior Tecnico, Universidade de Lisboa*, 2014.

[11] Davide Piciucco. Bayesian forces identification in cable networks with small bending stiffness. Master's thesis, Politecnico di Milano, 2020-2021.

[12] Ilker Yildirim. Bayesian inference: Metropolis-hastings sampling. *University of Rochester*, 2012.